Speech-in-noise intelligibility difficulties with age: the role of cochlear synaptopathy

Markus Garrett[1†‡], **Viacheslav Vasilkov**[2†§], **Manfred Mauermann**[1‡], **John L. Wilson**[3,5], **Kenneth S. Henry**[3,4,5], **Sarah Verhulst**[2§]

***For correspondence:** s.verhulst@ugent.be ( )

[†]These authors contributed equally to this work

Present address: [‡]Carl-von-Ossietzky-Straße 9-11, 26129, Oldenburg, Germany; [§]Technologiepark 126, 9052 Zwijnaarde, Belgium

[1]Medizinische Physik and Cluster of Excellence "Hearing4all", Department of Medical Physics and Acoustics, Carl von Ossietzky University of Oldenburg, DE; [2]Hearing Technology @ WAVES, Department of Information Technology, Ghent University, BE; [3]Department of Otolaryngology, University of Rochester, Rochester, NY USA; [4]Department of Biomedical Engineering, University of Rochester, Rochester, NY USA; [5]Department of Neuroscience, University of Rochester, Rochester, NY USA

Abstract Damage to auditory-nerve-fiber synapses (i.e. cochlear synaptopathy) degrades the neural coding of sound and is predicted to impair sound perception in noisy listening environments. However, establishing a causal relationship between synaptopathy and speech intelligibility is difficult because we have no direct access to synapse counts in humans. Hence, we rely on the quality of noninvasive auditory-evoked potential (AEP) markers developed in rodent studies of histologically-verified synaptopathy. However, there are a number of reasons which render the interpretation of these markers in humans difficult. To bridge this translational gap, we apply a multi-method approach to enable a meaningful interpretation of the relationship between the histopathology of sensorineural hearing loss (SNHL) and speech perception. We first selected a synaptopathy-sensitive AEP marker and verified its sensitivity (i) in an animal model using a Kainic-acid induced synaptopathy, and (ii), via auditory model simulations which connect the histopathology of SNHL to the source generators of AEPs. Secondly, we restricted the frequency content of the speech-material to ensure that both AEP and speech metrics targeted similar cochlear frequency regions and associated auditory coding mechanisms. Following this approach, we studied the relative contribution of AEP markers of synaptopathy and hearing sensitivity to speech recognition thresholds in 44 listeners (24 women) of different ages and SNHL profiles. Our analysis shows that synaptopathy plays an important role for speech intelligibility in noise, but that outer-hair-cell integrity predicts performance in the absence of noise. Our results corroborate conclusions from animal studies regarding the prevalence of age-related synaptopathy, and its occurrence before outer-hair-cell loss damage.

Significance Statement

Temporal-bone histology demonstrates that cochlear synaptopathy, i.e. damage to inner-hair-cell auditory-nerve fiber synapses, sets in before sensory cell damage and associated hearing threshold elevation. Clinical practice assesses hearing status on the basis of audiometric thresholds, and is hence overlooking a -likely prevalent- aspect of sensorineural hearing damage given that ageing, noise exposure or ototoxic drugs can cause synaptopathy. We present a multi-method approach to study the relationship between synaptopathy and speech intelligibility and address an important

unresolved issue in hearing science, namely why speech-intelligibility-in-noise degrades as we age, even when hearing sensitivity remains normal. Our study outcomes have important implications for hearing diagnostics and treatment.

Abbreviations

AN(F) - auditory nerve (fiber);
BB - broadband;
CF - characteristic frequency;
CN - cochlear nucleus;
DPOAE - distortion product otoacoustic emission;
EEG - electroencephalography;
EFR - envelope following response;
H/M/LSR fibers - high/medium/low spontaneous rate fibers;
HI - hearing-impaired;
HP - highpass filtered;
IC - inferior colliculus;
IHC - inner hair cell;
IQR - interquartile range;
ISI - Inter stimulus interval;
I/O function - input/output function;
LP - lowpass filtered;
NH - normal-hearing;
OHC - outer hair cell;
peSPL - peak-equivalent sound pressure level;
PT - pure-tone;
SAM - sinusoidally amplitude-modulated;
SiN - speech in noise;
SiQ - speech in quiet;
SNHL - sensorineural hearing loss;
SPL - sound pressure level;
RAM25 - rectangularly amplitude-modulated with 25% duty cycle;
TENV - temporal envelope;
TFS - temporal fine structure;

Introduction

The cochlea is deeply embedded within the temporal bone, rendering a direct assessment of sensorineural hearing loss (SNHL) impossible in living humans. While outer-hair-cell (OHC) deficits are routinely diagnosed using indirect metrics such as the pure-tone-audiogram or distortion-product-otoacoustic-emission (DPOAE) threshold, damage to auditory-nerve-fiber (ANF) synapses between the inner hair cells (IHCs) and spiral ganglion cells, i.e., *cochlear synaptopathy* (***Kujawa and Liberman, 2009***), can so far only be quantified via post-mortem temporal bone histology (***Makary et al., 2011***; ***Viana et al., 2015***; ***Wu et al., 2018***). Synaptopathy compromises temporal envelope (TENV) coding of supra-threshold stimuli, as observed through reduced envelope-following responses (EFRs) in animals with histologically verified synaptopathy (***Parthasarathy et al., 2014***; ***Shaheen et al., 2015***; ***Parthasarathy and Kujawa, 2018***). The EFR is an indirect and non-invasive auditory-evoked potential (AEP) metric which reflects the phase-locked neural response of a population of

peripheral and brainstem neurons to a stimulus envelope (***Kraus et al., 2017***), and its frequency-domain response exhibits peaks coinciding with the stimulus modulation frequency and its harmonics. Given that EFRs can be recorded reliably in both animals and humans, its spectral magnitude has been proposed as a non-invasive marker of synaptopathy which can be used across species. Synaptopathy occurs before hearing sensitivity is compromised (***Sergeyenko et al., 2013***; ***Fernandez et al., 2015***; ***Parthasarathy and Kujawa, 2018***) and impacts supra-threshold sound coding, hence it is believed to play a role in the hitherto unexplained observation that the audiogram does not predict speech recognition performance in noise (***Festen and Plomp, 1983***; ***Papakonstantinou et al., 2011***).

However, existing studies which investigated the relation between the EFR and sound perception have led to a corpus of mixed and inconclusive results (e.g. ***Bharadwaj et al., 2015***; ***Grose et al., 2017***; ***Prendergast et al., 2017***; ***Guest et al., 2018***; ***Johannesen et al., 2019***). A combination of factors could be responsible: (i) individual differences in absolute EFR strength can, to a certain degree, reflect non-hearing-related factors in humans (***Trune et al., 1988***; ***Mitchell et al., 1989***; ***Plack et al., 2016***) and require a relative metric design (e.g. ***Bharadwaj et al., 2015***; ***Mehraei et al., 2016***; ***Hickox et al., 2017***; ***Le Prell, 2019***). (ii) As the EFR can reflect a mixture of synaptopathy and OHC deficits, an unambiguous interpretation of the EFR in terms of synaptopathy is difficult when the histopathology is unknown (***Garrett and Verhulst, 2019***; ***Vasilkov and Verhulst, 2019***). (iii) The recording paradigms established in animal studies might not be sensitive enough for application in humans and hence overlook synaptopathy (***Hickox et al., 2017***; ***Bramhall et al., 2019***). Lastly, (iv) whereas speech is a broadband signal, the EFR mostly reflects auditory TENV coding mechanisms associated with ANF fibers above the phase-locking limit (***Joris and Yin, 1992***; ***Verschooten et al., 2015***; ***Henry et al., 2016***). Speech recognition also depends on the frequency content below the phase-locking limit, which is encoded as temporal fine-structure (TFS) information by the ANFs, and which is a strong perceptual cue (e.g. ***Lorenzi et al., 2006***; ***Hopkins et al., 2008***; ***Hopkins and Moore, 2010***; ***Henry et al., 2016***). TFS coding is, however, not targeted by conventional EFR markers which predominantly reflect TENV coding mechanisms and their impairments. Hence, a missing correlation between the EFR to high-frequent carriers and speech recognition does not necessarily reflect an absence of synaptopathy, but can also occur when separate mechanisms drive individual performance in either metric.

In this study, we address the factors which have rendered an interpretation of the relation between speech perception and EFR markers of synaptopathy difficult. First, we selected an optimized EFR marker and applied it in a relative metric design to yield a strong EFR which captures individual synaptopathy differences (***Vasilkov et al., 2020***). The sensitivity of the marker to synaptopathy, in absence and presence of OHC deficits, was tested using simulations with a computa-

tional model of the auditory periphery (***Verhulst et al., 2018a***; ***Osses Vecchi and Verhulst, 2019***, v1.2). We furthermore confirmed in an animal (budgerigar) model of selective ANF damage that this new marker is more robust than conventionally adopted EFR-based synaptopathy markers and that it is strongly reduced after Kainic-Acid administration. We then evaluated the relationship between the EFR marker and speech intelligibility for low and high-pass filtered speech material. We hypothesize that individual differences in EFR marker strength predict speech recognition thresholds better when both rely on cochlear TENV mechanisms (and their impairments). To identify the respective role of synaptopathy and hearing sensitivity for speech intelligibility, we studied the relationships between objective markers of hearing and speech intelligibility in young normal-hearing listeners and two age-matched groups of older participants with normal or impaired audiograms. We assume that the older listeners suffer from age-related synaptopathy (***Wu et al., 2018***) with possible co-existing OHC damage pathologies.

The primary goal of this study was to estimate the unique and common contributions of OHC damage and synaptopathy to word recognition scores. Based on collected data from three participant groups, we evaluated whether group and individual differences in EFR strength, DPOAE threshold and their relationship to speech recognition in quiet and in noise are consistent with how cochlear synaptopathy is believed to affect auditory function. Specifically, we tested the following hypotheses:

1. Restricting the frequency spectrum of the speech material to frequencies above the ANF phase-locking limit confines the speech task to rely on high-frequency coding mechanisms (i.e., TENV and audibility). This ensures a better match between targeted coding mechanisms across speech and EFR markers of synaptopathy. Consequently, we expect that the correlation strength between the EFR and speech recognition will be stronger in this configuration than when using unfiltered or low-pass filtered speech, the latter relying on both TFS+TENV or TFS coding mechanisms respectively.
2. Our model simulations suggest that the EFR stimulus envelope can be optimized to emphasize inter-individual differences in EFR strength (***Vasilkov et al., 2020***). The sensitivity of the new EFR metric to synaptopathy, and its overall larger response strength than the classically adopted sinusoidally amplitude-modulated (SAM) EFR, should be confirmed in an animal model of Kainic-acid induced synaptopathy. Secondly, our model simulations showed that for an optimal EFR stimulation paradigm, the EFR strength is largely independent from the degree of OHC damage (***Vasilkov et al., 2020***), our human EFR recordings should be consistent with this trend.
3. Assuming that synaptopathy plays a role in speech-in-noise intelligibility, we expect to see a strong correlation between EFR strength and the speech reception threshold. At the same

time, this relationship should become weaker when evaluating speech recognition in quiet as the latter task is well-known to rely on hearing sensitivity (***Festen and Plomp, 1983***). Motivation for a presumable role for synaptopathy in speech-in-noise, but not speech-in-quiet, intelligibility stems from a stochastic undersampling principle (***Lopez-Poveda and Barrios, 2013***; ***Lopez-Poveda, 2014***; ***Marmel et al., 2015***), by which a sufficient number of ANF fibers is necessary to encode a stimulus in noise reliably. Additionally, the effective dynamic range of ANF coding is reduced when stimuli are presented in a noise background (***Costalupes et al., 1984***; ***Huet et al., 2016***), which provides another explanation as to why an intact ANF population might be important for speech-in-noise processing.

To interpret individual EFR differences in terms of synaptopathy, we complemented our human data-collection with recordings from a Kainic-acid animal model of synaptopathy (***Henry and Abrams, 2018***), as well as with model simulations which can - from a basic understanding of the physiology of hearing (damage) - predict how different aspects of SNHL affect the generators of EFRs in humans. This multi-method approach is crucial given that direct histopathological evidence for the relationship between synaptopathy and EFR strength presently only exists in lab animals.

Materials and Methods

Study Participants

Three participant groups were recruited using age (20 ≤ age ≤ 30 or 60 ≤ age ≤ 70) and audiometric pure-tone thresholds (≤ or > 25 dB HL for frequencies up to 4 kHz) as the classification criteria. This grouping criterion did not consider individual degrees of synaptopathy which is an unknown variable. Fifteen young normal-hearing (yNH: 24.5 ± 2.3 y/o, 8 females), 16 older normal-hearing (oNH: 64.3 ± 1.9 y/o, 8 females) and 13 older hearing-impaired (oHI: 65.2 ± 1.8 y/o, 8 females) participants took part in the study. There were no significant age differences between the oNH and oHI participant groups ($t_{(27)}$ = -1.41, p = 0.17). Otoscopy was performed prior to data collection to ensure that participants had no obstructions or other visible pathologies. The experiments were approved by the ethics committee of the University of Oldenburg. Participants gave written informed consent and were paid for their participation.

Pure-tone audiometric thresholds (PTs) were collected for frequencies between 0.125-8 kHz using Sennheiser HDA200 headphones and a clinical audiometer AT900 (Auritec). Figure 1 shows audiograms of the audiometrically better ear (right ear - yNH: 10, oNH: 11, oHI: 10) which was used for testing. Normal-hearing participants had mean (± std) 4-kHz pure-tone thresholds of 3.3 ± 3.6 (yNH) and 11.6 ± 4.0 dB HL (oNH) respectively. The oHI group had high-frequency sloping audiograms with 4-kHz thresholds of 37.7 ± 6.7 dB HL.

Distortion-product otoacoustic emissions (DPOAEs) were recorded at 4 kHz to yield a more direct assessment of OHC integrity and cochlear function than offered by the behavioral audiogram. DPOAE stimuli were presented over ER-2 speakers using foam ear tips and recordings were made using the ER10B+ OAE microphone system (Etymotic Research) and custom-made MATLAB scripts (***Mauermann, 2013***). Two pure tones (f_1, f_2) were simultaneously presented at a fixed f_2/f_1 ratio of 1.2 using a primary frequency sweep method (***Long et al., 2008***). Frequencies were exponentially swept up (2 s/octave) over a 1/3rd octave range around the geometric mean of 4 kHz. L_1 levels followed the Scissors paradigm (L_1=0.4 L_2+39; ***Kummer et al., 1998***) given a primary L_2 level of 30-60 dB SPL in steps of 6 dB (in oHI listeners, L_2s of 66 and 72 dB SPL were additionally collected). The distortion component (L_{DC}) was extracted using a sharp least-squares-fit filter of 2 Hz and the center frequency of the measured frequency range was used to construct L_{DC} growth functions. Individual L_{DC} data points and their standard deviations were used in a bootstrapping procedure to fit an adapted cubic function through the L_{DC} datapoints as described in ***Verhulst et al.*** (***2016***). It is generally assumed that the recorded L_{DC} growth functions monotonically increase with L_2, when the DPOAE generators are of OHC origin. Non-monotonous growth functions were hence assumed to be contaminated by additional distortion components or noise (see ***Mauermann and Kollmeier, 2004***). To impose monotonous growth on each bootstrap run L_{DC} (L_2,b), we used an automated algorithm which eliminated adjacent data points at either end of the growth function (never intermediate points) that compromised monotonicity. DPOAE thresholds were determined as the median of the bootstrapped levels of L_2 at which the extrapolated fitting curve reached a level of -25 dB SPL as for the two-slope fit in ***Neely et al.*** (***2009***). Two yNH participants with reasonable growth functions but very low thresholds (-30.9, -5.4 dB SPL) were set to 1.5-times the interquartile range (IQR) of the yNH-DPOAE threshold distribution (-4.3 dB) to avoid high-leverage data-points. 4-kHz audiometric and DPOAE thresholds are depicted in Figure 2 and show similar patterns across groups and a significant correlation between measures (ρ = 0.84; $p < 0.0001$, n = 44), in agreement with a large population study (***Boege and Janssen, 2002***).

Individual speech reception thresholds (SRTs)

To assess how speech intelligibility is compromised when listening in noise, we applied a standard German Matrix test to determine the speech reception threshold (SRT) in quiet or in a fixed-level noise background (Matrix-test or OLSA; ***Wagener et al., 1999***; ***Brand and Kollmeier, 2002***). The OLSA test consists of natural 5-word sentences (male speaker: name - verb - numeral - adjective - object) using a corpus of 50 possible words. The speech-shaped background noise (SSN) was generated from the sentences and matched the long-term spectrum of the speech material. The speech recognition threshold for 50% correctly identified words (SRT_{50}) was determined using a 1-up/1-down adaptive procedure with varying step size based on word scoring (20 sentences per

condition). We expect that the fixed level background noise (i) compromises speech coding redundancy through the deafferentation principle (***Lopez-Poveda and Barrios, 2013***), while (ii) having listeners rely on supra-threshold ANF integrity and TENV coding, known to be compromised after synaptopathy (***Shaheen et al., 2015***; ***Parthasarathy and Kujawa, 2018***).

The SRT_{50} was determined in quiet (SiQ) and noise (SiN) for unfiltered/broadband speech (BB), low-pass filtered speech (LP) and high-pass filtered speech (HP). The idea behind using filtered sound stimuli, is that the LP condition would predominantly rely on low-frequency TFS mechanisms, while the HP condition would mostly rely on high-frequency TENV mechanisms since phase-locking to TFS declines with increasing frequency (i.e., 1.4 kHz in humans based on ITD sensitivity; ***Joris and Verschooten, 2013***). The speech and noise signals in the LP and HP conditions were generated by applying a 1024th order FIR filter with respective cut-off frequencies of 1.5 and 1.65 kHz (***Verhulst and Warzybok, 2019***). The initial speech level was 70 dB SPL and the noise level was kept fixed at 70 dB SPL while the speech level varied adaptively to yield the SRT_{50} in the SiN conditions. All six conditions (3 SiQ, 3 SiN) were presented in pseudo-random order. Participants completed three training runs in which a SiN_{BB} with a fixed SNR of 5 dB was followed by a regular SiN_{BB} condition with SRT_{50} tracking for training purposes. All possible words were displayed on the screen during those runs to familiarize participants with the stimulus material. The third training run was a SiN_{HP} condition with SRT_{50} tracking but without visual aid. During the experiment, answers were logged by the experimenter and no visual feedback was provided. Measurements were conducted in a double-walled sound-insulated booth using Sennheiser HDA200 headphones in combination with the Earbox Highpower ear 3.0 sound card (Auritec) and the Oldenburg Measurement Platform (HörTech gGmbH). The setup was calibrated using an artificial ear type 4153, microphone type 4134, preamplifier type 2669 and sound level meter type 2610 (Brüel & Kjær).

EFR stimuli

EFRs were recorded to two amplitude-modulated pure-tone stimuli with the same carrier frequency (f = 4 kHz) and rate (f_m = 120 Hz, starting phase (φ) of $\frac{3\pi}{2}$). The only difference between the stimuli was their envelope shape: the SAM stimulus had a sinusoidal modulator (Eq.1) while the second modulator was a rectangular-wave with a duty-cycle (τ) of 25% (RAM25; ***Vasilkov et al., 2020***). A modulation depth (md) of 0.95 (95%, -0.45 dB re. 100%) was used. MATLAB's 'square' function was adopted to create the RAM25 stimulus, and both stimuli can be described as follows:

$$SAM\ :\ x(t) = \left[1 + md \cdot \sin\left(2\pi f_{\mathrm{m}} t + \varphi\right)\right] \sin\left(2\pi f t\right) \tag{1}$$

$$RAM25: \; y(t) = [2 + 2md \cdot m(t)] \sin(2\pi f t), \text{ with}$$
$$m(t) = 2 \sum_{n=0}^{d \cdot f_m - 1} \left[u\left(t \cdot f_m - n + \frac{\varphi}{2\pi}\right) - u\left(t \cdot f_m - n + \frac{\varphi}{2\pi} - \tau\right)\right] - 1, \text{ and} \tag{2}$$
$$u[p] = \begin{cases} 0, p < 0, \\ 1, p \geq 0, \end{cases} \quad \text{(unit step function)}$$

Figures 3A and B depict two cycles of each stimulus type. Both stimuli were windowed using a 2.5% tapered-cosine window, had a duration (d) of 0.4 seconds and were repeated 1000 times each (500 per polarity). The inter stimulus interval (ISI) consisted of a uniformly distributed random silence jitter (mean ISI: 100 ms ± 10 ms). The SAM tone was presented at 70 dB SPL and the RAM25 stimulus was presented at the same peak-to-peak amplitude, which corresponded to 68 dB SPL. In a separate study, we recorded, evaluated and simulated a broad range of possible electrophysiological markers of synaptopathy (***Vasilkov et al., 2020***) and we selected the most promising RAM25-EFR stimulus for use in the present study.

EFR recordings and analysis

EEG recordings took place in a double-walled electrically shielded measurement booth (IAC acoustics) and participants sat in a reclining chair while watching a silent movie. EEGs were measured using a 64-channel cap with equidistant electrode spacing (Easycap) and active Biosemi Ag/AgCl electrodes were connected to a Biosemi amplifier. A sampling rate (f_s) of 16384 Hz and 24-bit AD conversion were used to store the raw data traces. A common-mode-sense (CMS) active electrode was placed on the fronto-central midline and a driven-right-leg (DRL) passive electrode was placed on the tip of the nose. Reference electrodes were placed on each earlobe. Electrode offsets (DC values of the common mode signal) were kept below 25 mV. Stimuli were generated in MATLAB (R2015b) at a sampling rate of 48 kHz and calibrated using the same equipment as for the speech recognition test (ear simulator type 4157 (Brüel & Kjær) for insert earphones). A Fireface UCX sound card (RME) and TDT-HB7 headphone driver (Tucker-Davis) were used to drive the ER-2 insert earphones (Etymotic Research) using the open-source portaudio playrec ASIO codec (***Humphrey, 2008***). Stimuli were presented monaurally based on the audiometrically better ear.

Raw EEG recordings were extracted in Python (version 2.7.10 | Anaconda 2.3.0 (64-bit), (www.python.org) and MNE-Python (version 0.9.0; ***Gramfort et al., 2013***, ***2014***) and all channels were re-referenced to the offline-averaged earlobe electrodes. Data were epoched in 0.4 s windows starting from the stimulus onset and baseline corrected by the average amplitude per epoch. We only present results from the vertex channel (Cz) in this study which is known to yield good signal strength for subcortical auditory sources (***Picton, 2010***).

Pre-processing was performed in MATLAB (R2014b). The EFR estimates for each stimulus condi-

tion and participant were computed based on the energy at the modulation frequency and its first four harmonics (h_0-h_4 = $k \times f_m$, k=[1..5]) to account for all envelope related energy in the EEG signal (***Vasilkov and Verhulst, 2019***). The mean EFR amplitude was estimated using Eq. 3 in a bootstrap routine (***Zhu et al., 2013***):

$$\begin{gathered}\mathrm{EFR_{PtN}} = \frac{peak\text{-}to\text{-}peak\left(\frac{1}{B}\sum_{b=1}^{B}\left(W_{\mathrm{b}}\right)\right)}{2}, \text{ with} \\ W_{\mathrm{b}} = \left(\frac{1}{N}\sum_{n=0}^{N-1}\left(\mathrm{F}_{n,b} - \mathrm{NF}_{n,b}\right)e^{i\theta_{n,b}}\right); \\ \text{if } n \neq \frac{k\mathrm{f}_m}{\mathrm{f}_s}N, \text{ then } \mathrm{F}_{n,b}, \mathrm{NF}_{n,b} = 0, \text{for } k = [1..5]\end{gathered} \tag{3}$$

N corresponds to the length of the magnitude spectrum. The process is visualized in Fig. 4. First, a mean spectral estimate of the neural response ($F_{n,b}$) for each frequency component (n) was computed by averaging the complex discrete Fourier transform (DFT) values of 1000 randomly drawn epochs using 500 epochs of each polarity (with replacement) in each bootstrap run (b). Epochs were windowed using a 2% tapered-cosine window before the frequency-domain transformation. The electrophysiological noise floor ($NF_{n,b}$) at frequencies h_0-h_4 was computed as the average magnitude of the ten frequency-bins surrounding the respective frequency (five bins each side). The noise floor estimates were then subtracted from the signal components h_0-h_4, to yield peak-to-noise floor ($PtN_{n,b}$) magnitude estimates (see Fig. 4A). If PtN values were negative, they were set to zero. All frequency components apart from the harmonic frequencies (h_0-h_4) were removed from the spectrum before it was transformed back to the time domain using the inverse DFT and the original phase information ($\theta_{n,b}$) of the harmonic frequencies. This procedure was repeated/bootstrapped to yield 200 (B) reconstructed time-domain estimates of the EFR waveform (W_b). The waveforms were averaged and the EFR was defined as half the peak-to-peak amplitude of the averaged reconstructed time-domain waveform (see Fig. 4B). The metric defined in Eq.3 is from here on referred to as the EFR peak-to-noise floor amplitude (EFR_{PtN}).

Post-hoc and statistical analysis

To disentangle the effects of synaptopathy and OHC damage on the EFR and speech metrics, we both considered the dataset as a whole ('ALL'), as well as performed a post-hoc grouping of participants into subgroups based on their suspected underlying mixtures of SNHL pathologies.

1. OLD: oNH and oHI participants were pooled into a single OLD group based on their age. This group is suspected to show similar degrees of age-related synaptopathy given their similar

and older age and outcomes of human temporal bone (***Wu et al., 2018***) and ageing studies (***Parthasarathy and Kujawa, 2018***). We expect to see a strong OHC integrity gradient among listeners within this group based on their hearing sensitivity differences.

2. NH_{DP}: Participants with 4-kHz DPOAE thresholds ≤ 25 dB SPL were pooled into a group with good OHC integrity. As by design, young and old participants could be assigned to this group, and hence we suspect to see a strong gradient in the degree of age-related synaptopathy among individuals within this group with comparable OHC integrity.
3. HI_{DP}: Participants with 4-kHz DPOAE thresholds > 25 dB SPL were assigned to this group. Mainly older participants with elevated hearing thresholds were part of this group. Based on outcomes from rodent studies, we expect that older listeners with elevated hearing thresholds also suffer from age-related synaptopathy which was shown to precede OHC damage in the ageing process (***Sergeyenko et al., 2013***; ***Parthasarathy and Kujawa, 2018***). Given that two young participants were also members of this group, the degree of synaptopathy is expected to vary among individuals within this group.

The 'SciPy' python package for scientific computing (***Oliphant, 2007***; ***Millman and Aivazis, 2011***) was used for two-sample inference statistics. All correlations reported refer to the Pearson correlation coefficient (r) if both variables were normally-distributed, otherwise the Spearman's rank correlation coefficient (ρ) was reported. The R programming environment (***R Core Team, 2019***) and 'lsmeans' package (***Russell, 2016***) was used for analyses of variance (ANOVA) and regression analyses. Reported p-values for multiple comparisons were Bonferroni adjusted to control for the family-wise error rate. Partial spearman correlation analyses were conducted using the 'PResiduals' package (***Dupont et al., 2018***) and partial pearson correlations were performed using the 'ppcor' package (***Kim, 2015***). Additionally, we performed commonality analysis using the 'yhat' package (***Nimon et al., 2008***). Commonality analysis combines linear regressions on the dependent variable and allows for the decomposition of the explained variance (R^2) of the linear predictors into subcomponents explained by the unique and the common/shared variance of predictors and all their possible combinations (***Newton and Spurrell, 1967***). This technique also works in the presence of multicollinearity (***Ray-Mukherjee et al., 2014***).

Model simulations of the EFR generators: impact of OHC damage and synaptopathy

To illustrate the sensitivity of the EFR marker to different aspects of SNHL, we adopted a computational model of the human auditory periphery (model implementation v1.2; ***Verhulst et al., 2018a***; ***Osses Vecchi and Verhulst, 2019***) to simulate how synaptopathy or OHC damage, separately and combined, affect the EFR strength. The model simulates how the ascending auditory pathway processes acoustic input, and includes middle-ear filtering, a nonlinear transmission-line representation of human cochlear mechanics (***Verhulst et al., 2012***; ***Altoè et al., 2014***), a biophysical model of the IHC-AN complex (***Altoè et al., 2018***), as well as a phenomenological description of ventral

cochlear nucleus (CN) and inferior colliculus (IC) neurons (***Nelson and Carney, 2004***). The model is suited for the purpose of this study as it accounts for human cochlear filter tuning characteristics (***Shera et al., 2010***; ***Verhulst et al., 2012***) and reasonably captures how OHC damage and synaptopathy affect human ABRs and EFRs for different sound intensities (***Verhulst et al., 2016***, ***2018a***). Note that the level-dependent properties of simulated ABRs and EFRs can be considered as a model outcome, i.e. they were not considered during the calibration procedure which was based on capturing cochlear and OAE properties as well as single-unit ANF responses.

EFRs were simulated by adding up activity across a tonotopic array of 401 IHC-AN/CN/IC units with characteristic frequencies (CFs) between 112 Hz and 12 kHz distributed according to the frequency-position map (***Greenwood, 1990***) at three processing stages: the AN (after summing up responses from 19 AN fibers synapsing onto single IHCs and across the simulated CFs; wave-I), the CN (wave-III) and IC (wave-V). Each simulated wave was scaled in amplitude according to normal-hearing human reference ABR data (Table 8-1 in ***Picton, 2010***; ***Osses Vecchi and Verhulst, 2019***) before they were added up to capture the different subcortical sources that contribute to the EFR (***Dolphin and Mountain, 1992***; ***Kuwada et al., 2002***).

SNHL was simulated by (i) implementing frequency-specific OHC damage, and (ii), changing the number and types of ANFs which innervate individual IHCs across the tonotopic range. We considered a flat 35-dB-HL audiogram (HI_{flat}) to simulate the effect of OHC damage on the EFR and implemented the loss by reducing the cochlear filter gain relative to the models' normal-hearing filter gain at low stimulus levels (in dB HL) across the simulated frequency range (***Verhulst et al., 2016***; ***Vasilkov and Verhulst, 2019***). The NH model had 19 ANFs synapsing onto each IHC: 13 high spontaneous-rate (HSR, 70 spikes/s), 3 medium spontaneous-rate (MSR, 10 spikes/s) and 3 low spontaneous-rate (LSR, 1 spike/s) fibers, following the empirical ratio observed in cats (***Liberman, 1978***). One profile with normal fiber integrity (13H,3M,3L) was simulated as well as three synaptopathy profiles in which the following fiber types were removed across the tonotopic axis: (i) all LSR and MSR fibers (13H,0M,0L), (ii) all LSR, MSR and 50 % of the HSR fibers (7H,0M,0L), and (iii) all LSR, MSR and 80 % of the HSR fibers (3H,0M,0L).

Sensitivity of the EFR to Kainic-acid induced synaptopathy

EFRs were also recorded in two young adult budgerigars (Melopsittacus undulatus), approximately two years of age, before and after induction of cochlear synaptopathy using kainic acid (KA). All procedures were performed at the University of Rochester and approved by the University Committee on Animal Resources. The budgerigar is a small parrot species with human-like behavioral sensitivity to many simple and complex sounds in operant conditioning studies (***Dent et al., 2000***; ***Dooling et al., 2000***), and was selected based on its use in ongoing behavioral studies of cochlear synaptopathy (***Wong et al., 2019***). KA is a glutamate analog that damages cochlear affer-

390 ent synapses between hair cells and auditory-nerve fibers through excitotoxicity in mammals and birds (***Bledsoe et al., 1981***; ***Pujol et al., 1985***; ***Zheng et al., 1997***; ***Sun et al., 2001***). In budgerigars, bilateral cochlear infusion of KA has been shown to permanently reduce ABR wave-I amplitude by up to 70% without impacting behavioral audiometric thresholds or distortion-product otoacoustic emissions generated by sensory hair cells (***Henry and Abrams, 2018***; ***Wong et al., 2019***). The
395 methods used to induce synaptopathy in budgerigars have been described previously (***Henry and Abrams, 2018***; ***Wong et al., 2019***). Briefly, animals were anesthetized with ketamine (5-6 mg/kg) and dexmedetomidine (0.1 mg/kg; subcutaneous bolus injection) and placed in a custom stereotaxic device. Ketamine/dexmedetomidine were administered subcutaneously for anesthetic induction, but anesthesia was maintained throughout the surgery (approximately 1-2 hours) by a continuous
400 anesthetic infusion pump (Razel Scientific; Fairfax, VT, USA). The middle-ear space was accessed surgically using a posterior approach to expose the basal prominence of the cochlear duct, where a 0.15-mm diameter cochleostomy was made using gentle rotating pressure on a small manual drill. Thereafter, 2.5 μL of 2-mM KA (Abcam ab 144490; Cambridge, UK) in hanks balanced salt solution (Sigma-Aldrich H8264; St. Louis, MO, USA) was infused into cochleostomy over 90 seconds using
405 a microinjection needle. Compound action potentials of the auditory nerve were recorded before and after infusion in response to clicks. Excitotoxic synaptic injury was confirmed by observing >90% reduction of compound action potentials within 10-20 minutes following KA exposure. The left and right ears were treated with KA during different surgical procedures four weeks apart to minimize operating time and to avoid excessive anesthetic exposure. Distortion-product otoacous-
410 tic emissions were recorded using a swept-tone paradigm (see ***Wong et al., 2019***) before and after surgeries to confirm no adverse impact of the procedures on sensory hair cells. Prior to KA exposure, wave-I amplitude of the ABR in response to 90-dB p.e. SPL clicks was 24.56 $\pm$ 2.31 μV in animal K20 and 23.69 $\pm$ 2.60 μV in animal K25 (means $\pm$ SD). Reduction of wave I, based on ABRs recorded four or more weeks post KA (during the steady-state period), was 68.5% in animal K20
415 and 64.9% in animal K25. EFRs were measured at two to three time points before kainic acid exposure at four time points after (4, 6, 8, and 12 weeks) the second infusion. Repeated measurements assessed within-subject variability of responses, since synaptic injury is relatively stable one month following KA exposure (***Sun et al., 2000***; ***Henry and Abrams, 2018***; ***Wong et al., 2019***). Anesthesia was performed as described above using ketamine and dexmedetomidine (for recording sessions,
420 anesthesia was only administered subcutaneously), and body temperature was maintained in the normal range for this species of 39-41 degrees C. Stimuli were generated in MATLAB (The MathWorks, Natick, MA, USA) at a sampling frequency of 50 kHz and converted to analog using a data acquisition card (PCIe-6251; National Instruments, Austin, TX, USA), which also digitized response activity using the same internal clock. Stimuli were presented free-field through a loudspeaker
425 (MC60; Polk Audio, Baltimore, MD, USA) positioned 20 cm from the animals head in the dorsal direction (the rostral surface of the head faced downward in the stereotaxic apparatus; thus the

loudspeaker and animal were located in the same horizontal plane). Level was controlled digitally (by scaling stimulus waveforms in MATLAB) and by up to 60 dB of analog attenuation applied by a programmable attenuator (PA5; Tucker Davis Technologies, Alachua, FL, USA). Calibration was based on the output of a $\frac{1}{4}$" precision microphone (model 4938; Brüel and Kjær, Marlborough, MA USA) in response to pure tones. Electrophysiological activity was recorded differentially between a stainless steel electrode implanted at the vertex (M0.6 threaded machine screw; advanced through the skull to the level of the dura) and a platinum needle electrode (model F-E2; Natus Manufacturing, Gort, Co. Galway, Ireland) inserted at the base of the skull near the nape of the neck. A second needle electrode in the animal's back served as ground. Activity was amplified by a factor of 50,000 and filtered from 30-10,000 Hz (P511; Grass Instruments, West Warwick, RI USA) prior to sampling (50 kHz) by the data acquisition card. Stimuli were SAM and RAM25 tones presented at 75 dB SPL with 10-ms cosine-squared onset and offset ramps, 300-ms duration, and a 130-ms silent interval between successive stimuli. Carrier frequency and modulation frequency were 2830 Hz and 100 Hz, respectively, and the polarity of the carrier signal was alternated between stimulus repetitions. Depth of modulation was 100%, and the duty-cycle for square wave modulation was fixed at 25%. Responses to 300 repetitions of the same stimulus (including both polarities) were averaged to produce each EFR waveform, following the procedure described in Eq.3.

Results

EFR sensitivity to synaptopathy and OHC deficits

Figures 3C,D depict simulated ANF firing rates from the combined ANFs which synapse onto a single IHC with a 4-kHz CF, i.e., the carrier frequency of the SAM and RAM25 stimulus (on-CF). Responses to two cycles of the SAM and RAM25 stimulus are shown for three SNHL profiles: (i) a NH response summed over 19 ANFs (NH), (ii) a synaptopathy response (HI_{synap}) in which the number of ANFs was reduced to seven high-SR fibers, and (iii) an OHC damage response (HI_{flat}) which had 19 ANFs and a hearing sensitivity loss of 35 dB across all frequencies.

In general, the RAM25 stimulus elicited a larger and more synchronized ANF response with sharper on- and off-sets compared to the SAM tone stimulus. The finding that faster rising stimulus-envelopes yield more synchronized ANF responses is discussed in detail in ***Vasilkov et al.*** (***2020***) and corroborates observations in single-unit ANF recordings (***Dreyer and Delgutte, 2006***). The ANF firing rate reduced for both stimulus types when a lower number of ANFs were available (white traces). Introducing OHC damage (orange traces) affected the responses to the SAM and RAM25 stimulus differently: while the ANF rate to the SAM tone was increased and started showing a bell-shaped pattern, the response to the RAM25 was barely affected. This outcome shows that on-CF ANF responses to the RAM25 stimulus are sensitive to the synaptopathy aspect of SNHL while being largely insensitive to the OHC damage aspect.

As scalp-recorded EFRs have more source-contributions than those stemming from the on-CF re-

gion alone (***Encina-Llamas et al., 2019***; ***Keshishzadeh et al., 2019b***), we also simulated population EFR responses in Fig. 5A. In agreement with the single unit responses, the simulated EFR_{PtN}s to the RAM25 stimulus (squares) were greater than the SAM-tone evoked EFR_{PtN}s (circles). Along with the overall increased EFR_{PtN} amplitudes, the RAM25 stimulus also yielded a greater sensitivity range. The predicted influence of OHC damage (HI_{flat}) was small compared to the effect of synaptopathy and became even smaller as the degree of synaptopathy increased.

Taken together, and explored in more detail in ***Vasilkov et al.*** (***2020***), the single-unit ANF and EFR_{PtN} simulations predict that the RAM25 stimulus (i) yields overall larger response amplitudes which could enhance the sensitivity of the EFR_{PtN} to characterize individual differences, and (ii) evokes a response which is primarily sensitive to synaptopathy, even when co-occurring OHC damage is present.

The kainic-acid manipulations performed in two budgerigars, which introduced selective AN damage without introducing OHC damage (normal DPOAEs), confirmed our model-predicted trends. (i) KA-induced synaptopathy reduced the mean bootstrapped SAM and RAM25-EFR waveforms in Fig. 3E,F considerably. (ii) Compared to the conventional SAM-EFR (Fig. 5C), the RAM25-EFR was about 2-2.5 times larger in the same animal before synaptopathy was introduced. Lastly, (iii), the same degree of synaptopathy shows a larger absolute reduction of the RAM25-EFR compared to the SAM-EFR in the same animal. This implies that RAM25-EFR amplitudes are more sensitive to identifying individual degrees of synaptopathy than the SAM-EFR amplitude.

Human EFR recordings: OHC and age-related deficits

The human EFR_{PtN} amplitudes depicted in Fig. 5B are in agreement with both model predictions (Fig. 5A) and animal-model findings (Fig. 5C) in showing larger overall RAM25 than SAM amplitudes (hypothesis #2). oNH listeners showed a mean 50% reduction of the RAM25 EFR amplitude, which worsened to 85% in the oHI group. Following the model simulations, this suggests a loss of 65% of all synapses in the first group (7H,0M,0L), which worsened to a 85 % loss (3H,0M,0L). These predicted damage percentages are high, but in range with findings of a temporal bone study which reported between 30 and 70% ANF loss in temporal bones of 60-70 year old humans ***Wu et al.*** (***2018***).

Secondly, the behavior of the oNH data across stimulus conditions may reflect sensitivity difference of the responses to different aspects of SNHL, as earlier discussed in ***Vasilkov et al.*** (***2020***). Whereas the oNH EFR_{PtN} results largely overlapped with those of the yNH group for the SAM stimulus (predicted to be sensitive to OHC and synaptopathy), there was a clear separation between the EFR_{PtN} amplitudes of the yNH and oNH groups to the RAM25 stimulus (predicted to be more sensitive to synaptopathy). To provide experimental support for the hypothesis that differences

between the yNH and oNH listeners were caused by age-related synaptopathy, we investigated to which degree EFR_{PtN} amplitudes were able to tell younger and older participants apart in groups of similar DPOAE thresholds. This grouping was necessary to ensure that the degree of OHC deficits was controlled for, while studying the EFR_{PtN} variability which was not related to hearing sensitivity.

Whereas it was not possible to discriminate between young and older NH_{DP} participants on the basis of the SAM-EFR_{PtN} (Fig. 6A), this separation was possible on the basis of the RAM25-EFR_{PtN}. The overall smaller SAM-EFR_{PtN} amplitudes could be the reason for this difference between stimuli, even though our simulations and the KA-data predicted that individual EFR_{PtN} differences to both stimulus types would predominantly reflect synaptopathy differences in the absence of overt OHC damage. The clear separation of NH_{DP} RAM25-EFR_{PtN} data into a younger and older participant group is consistent with how age-related synaptopathy affects the EFR amplitude in rodents (***Sergeyenko et al., 2013***; ***Fernandez et al., 2015***; ***Möhrle et al., 2016***; ***Parthasarathy and Kujawa, 2018***).

If age-induced synaptopathy was indeed the factor driving the human RAM25-EFR_{PtN} amplitudes (hypothesis #2), they should also be able to separate older from younger participants in the HI_{DP} group. Figure 6B,D confirms this possibility and shows that older listeners consistently had lower EFR_{PtN} amplitudes. These reductions could not be explained on the basis of their DPOAE thresholds alone, given that young and older listeners with DPOAE thresholds between 25 and 40 dB SPL covered the entire range of EFR_{PtN} amplitudes. Lastly, the two younger participants with elevated DPOAE thresholds had different SAM-EFR_{PtN} amplitudes but similar RAM25-EFR_{PtN} amplitudes. This different response to the two stimuli could be attributed to the reduced sensitivity of the RAM25 stimulus to OHC damage as compared to the SAM stimulus, whereby individual OHC-damage differences would be factored out better in the RAM25-EFR_{PtN}, but not SAM-EFR_{PtN} results.

The combined simulation and experimental approach shows that the RAM25 stimulus is a sensitive marker of synaptopathy and that it captures age-related, rather than OHC-damage, aspects of SNHL. Going further, we will evaluated to which degree EFR markers of synaptopathy predict speech reception thresholds.

Speech recognition thresholds: group differences

Individual and group SRTs are depicted in Figure 7 for the SiQ and SiN conditions. A two-factor (3x3) mixed design ANOVA was applied to investigate the roles of participant group and filter-condition on the SRT_{50}. Apart from significant main effects of group (SiQ: $F_{(2,41)} = 33.43$, $p < 0.0001$; SiN: $F_{(2,41)} = 35.66$, $p < 0.0001$) and filter-condition (SiQ: $F_{(2,82)} = 505.76$, $p < 0.0001$; SiN: $F_{(2,82)} = 747.20$, $p < 0.0001$), the interaction terms were also significant (SiQ: $F_{(4,82)} = 31.71$, $p < 0.0001$; SiN: $F_{(4,82)} = 20.93$, $p < 0.0001$), indicating that the groups were differently affected by the filtering.

If SiN performance is predominantly driven by synaptopathy, and SiQ performance by hearing

sensitivity (hypothesis #3), the group SRTs should reflect these differences. The SiQ SRT should be different between the groups (i.e. following the gradual decrease of hearing sensitivity, Fig. 1), whereas the SiN SRT should be more similar between oNH and oHI groups given that both might suffer from age-related synaptopathy. We standardized the SiQ and SiN SRT_{50} using z-scores to include the effect of adding SSN in a (3x6) mixed design ANOVA and we complemented this analysis with post-hoc pairwise comparisons. The post-hoc analysis showed significant differences between all three groups in the $SRT_{SiQ\text{-}HP}$ condition ($7.12 \leq$ t-ratio ≤ 14.19, $p < 0.0001$) and this difference disappeared between the oNH and oHI groups in the $SRT_{SiN\text{-}HP}$ condition (t-ratio = 3.56, $p = 0.15$), in agreement with our hypothesis #3. The only significant group difference in the LP and BB conditions was found in the quiet condition and between the yNH and oHI participants ($SRT_{SiQ\text{-}BB}$: t-ratio = 4.72, $p = 0.0042$). Group differences were generally smallest for the LP conditions when compared to the BB and HP conditions (particularly in noise). Our results show that providing only high-frequency speech content, was most effective to reveal SRT_{50} group differences. Furthermore, adding noise affected the SRT_{50} in the oNH listener group particularly strongly, to the extent that their performances aligned with that of oHI participants. Our observations fall in line with how OHC damage and synaptopathy are expected to influence speech understanding in quiet and noise, respectively (hypothesis #3). Whereas synaptopathy was the factor limiting the SiN performance, OHC damage was the factor limiting the SiQ performance.

Speech reception thresholds: individual differences

To test whether synaptopathy drives individual SRT performance, it is necessary that the speech task targets the same cochlear frequency range and coding mechanisms as is targeted by the EFR marker. We only provided high-frequency content of the speech material to achieve this goal, and consequently expect that individual RAM25-EFR_{PtN} amplitudes are a better predictor for the HP SRT_{50} than for the BB SRT_{50} or LP SRT_{50} (hypothesis #1). As the LP SRT_{50} condition particularly minimizes the contribution of high-frequency TENV coding to perception, we expect to find a strongly reduced relationship between LP SRT_{50} and the EFR markers. Relationships between the EFR_{PtN} and SRT_{50} are depicted in Figure 8, and confirm that EFR_{PtN} amplitudes predicted the SRT_{50} scores best when HP filtered stimuli were used (C/D) and do not predict the scores in the LP condition (B/E). Secondly, the RAM25 stimulus was a better predictor of the SRT_{50} scores (D/E/F) than the SAM stimulus (A/B/C). The overall increased RAM25-EFR_{PtN} amplitudes resulted in a wider spread of individual EFR data, and consequently became a strong predictor of the SRT_{50} in the NH_{DP} and ALL groups. These findings show that an objective and sensitive marker of synaptopathy predicts speech recognition performance in noise across participants of different ages who either had normal or elevated hearing thresholds. However, whether this relationship was caused by synaptopathy simultaneously reducing the RAM25-EFR_{PtN} amplitude and increasing the SRT_{50} in the same individuals, remains questionable until other aspects which could confound this relationship are

ruled out. Confounding factors relate to aspects which only impact speech intelligibility but not the RAM25-EFR$_{PtN}$ metric, or may point to a dominance of other inter-correlated SNHL pathologies (e.g. OHC damage) which could drive both the metrics in the relationship. The following sections further explore these aspects.

The role of OHC damage in predicting the SRT$_{SiN\text{-}HP}$

As permanent OHC damage is preceded by synaptopathy in the general ageing process (***Sergeyenko et al., 2013***; ***Fernandez et al., 2015***; ***Parthasarathy and Kujawa, 2018***) or after noise exposure (***Kujawa and Liberman, 2009***; ***Furman et al., 2013***), markers of OHC damage might also be a predictor of synaptopathy. Even though these two pathologies are unrelated in their pathogenesis and differ in their consequences on auditory processing, they share some of the same risk factors (e.g. age, noise exposure) and can both have an impact on EFR strength (***Garrett and Verhulst, 2019***). So even if the RAM25-EFR marker primarily captures synaptopathy-related information (as the model simulations and KA-manipulations predict), its strength might still relate to auditory threshold measures if people with impaired audiograms also suffer from synaptopathy. At the same time, the SRT$_{50}$ performance can also be affected by synaptopathy and OHC damage (***Hoben et al., 2017***; ***Holmes and Griffiths, 2019***), the latter aspect known to result in compromised frequency selectivity (***Glasberg and Moore, 1986***). To factor out the mediating effect of OHC damage on the relationship between the SRT$_{SiN\text{-}HP}$ and RAM25-EFR$_{PtN}$ amplitude, we computed partial correlation coefficients which controlled for the influence of the 4-kHz DPOAE threshold (TH$_{DPOAE,4kHz}$) as a marker of OHC-damage (***Davis et al., 2005***). The partial correlation yielded a smaller, but still significant, relationship between the RAM25-EFR$_{PtN}$ and SRT$_{SiN\text{-}HP}$:($\rho_{\mathrm{RAM25-EFR_{PtN}\ SRT_{SiN-HP}\cdot TH_{DPOAE,4kHz}}}$ = -0.44, p < 0.007, n = 44) when considering all participants. For the NH$_{DP}$ subgroup, the influence of the DPOAE threshold on the relationship was expected to be small and the partial correlation confirmed this by only marginally decreasing ($r_{\mathrm{RAM25-EFR_{PtN}\ SRT_{SiN-HP}\cdot TH_{DPOAE,4kHz}}}$ = -0.72, p = 0.0008, n = 19). Conversely, the correlation disappeared completely for the OLD subgroup ($\rho_{\mathrm{RAM25-EFR_{PtN}\ SRT_{SiN-HP}\cdot TH_{DPOAE,4kHz}}}$ = -0.0, p = 0.994, n = 29), suggesting that in the presence of similar degrees of suspected synaptopathy, the weak correlation could be explained by the mediating effect of OHC loss on both metrics. Secondly, to investigate possible collinearity between the RAM25-EFR$_{PtN}$ amplitude and DPOAE threshold, we ran a multiple linear regression model and commonality analysis, which controlled for OHC damage by adding the DPOAE threshold as a covariate. We assumed a basic additive model because adding an interaction term did not improve the model predictions significantly ($F_{(1,40)}$ = 0.74, p = 0.4):

$$\mathrm{SRT_{SiN\text{-}HP}} = \beta_0 + \beta_1 * \mathrm{RAM25\text{-}EFR_{PtN}} + \beta_2 * \mathrm{TH_{DPOAE,4kHz}} + \epsilon. \tag{4}$$

Results for all participants (ALL) as well as the NH$_{DP}$ and OLD subgroups are summarized in Table 1.

Table 1

Group	R^2	Adj. R^2	F (df_1,df_2)	p	beta	unique	common
ALL	0.55	0.53	24.76 (2,41)	<0.0001	β_1=-23.65***	30.37%	58.38%
					β_2=0.06*	11.26%	
NH_{DP}	0.56	0.51	10.23 (2,16)	0.0014	β_1=-25.89***	82.59%	15.18%
					β_2=0.03	2.22%	
OLD	0.12	0.05	1.73 (2,26)	0.1969	β_1=-9.18	13.13%	50.92%
					β_2=0.04	35.95%	

Signif. codes: 0 '***' 0.001 '**' 0.01 '*' 0.05 '.' 0.1 ' ' 1

Across participants (ALL), we observed a strong dependence of both predictors which shared the majority of the explained variance. However, even in the presence of mixed pathologies, the RAM25-EFR_{PtN} showed the largest unique explanatory effect on the $SRT_{SiN\text{-}HP}$ performance. For the NH_{DP} group, the RAM25-EFR_{PtN} explained nearly half the total $SRT_{SiN\text{-}HP}$ variance, in line with our prediction that the degree of synaptopathy would play a dominant role for SiN recognition when hearing sensitivity is normal (hypothesis #3). In contrast, the model for the OLD group was not significant, and points to similar degrees of age-related synaptopathy in these age-matched groups and a low predictive effect of OHC damage for high-pass filtered speech-in-noise performance. Our analysis shows that the RAM25-EFR_{PtN} metric is able to capture considerably large unique portions of the variance in $SRT_{SiN\text{-}HP}$ scores, which we - via our modeling work and KA manipulations - can relate to individual degrees of synaptopathy. Our results are also concordant with how synaptopathy is expected to influence speech-in-noise performance in the investigated groups.

The role of age in predicting the $SRT_{SiN\text{-}HP}$

To exclude the possibility that age-related factors, unrelated to synaptopathy, explain the observed RAM25-EFR_{PtN} amplitude differences within the different age groups, we performed a correlation analysis which showed that age alone was a poor predictor for the RAM25-EFR_{PtN} (yNH: r = -0.1, p = 0.73; n = 15; OLD: ρ = -0.15, p = 0.44; n = 29). Nevertheless, on a more general level, age is associated with the development of both OHC damage (***Lin et al., 2011***; ***ISO, 2017***) and synaptopathy (***Schmiedt et al., 1996***; ***Makary et al., 2011***; ***Konrad-Martin et al., 2012***; ***Möhrle et al., 2016***; ***Parthasarathy and Kujawa, 2018***) and can hence be responsible for the observed stronger age vs RAM25-EFR_{PtN} relationship when pooling the data across groups (ρ = -0.66, p < 0.0001; n = 44). The interplay between age and the development of hearing deficits can be further illustrated by adding the age-variable (+β_3*age) to the regression model in Eq.4. The resulting model for all participants (ALL: $F_{(1,40)}$ = 9.36, p = 0.004) and the NH_{DP} subgroup ($F_{(1,15)}$ = 17.02, p = 0.0009) were significantly improved by adding the age-variable, but are misleading due to the strong collinearity between age and all other

predictors (RAM25-EFR$_{PtN}$, TH$_{DPOAE,4kHz}$) as reflected in the commonality coefficients. All unique contributions were small compared to the fraction of the model's total explained variance captured by common effects associated with age (i.e., ALL: 58.76 out of 63.29% total variance; NH$_{DP}$: 74.23 out of 79.44% total variance). This demonstrates that age is inherently linked to *all* considered facets of SNHL but that for this reason, its inclusion in statistical models exacerbates the interpretation of the unique underlying effects of synaptopathy and OHC damage. Lastly, when calculating partial correlation coefficients between RAM25-EFR$_{PtN}$ and SRT$_{SiN\text{-}HP}$ and controlling for TH$_{DPOAE,4kHz}$ and age, the model still explained 20% of the total SRT$_{SiN\text{-}HP}$ variance among participants of the NH$_{DP}$ subgroup ($r_{\mathrm{RAM25-EFR_{PtN}}\ \mathrm{SRT_{SiN-HP}}\cdot \mathrm{TH_{DPOAE,4kHz}},\ \mathrm{age}}$ = -0.45, p = 0.073; non-significant). Taken together, we conclude that age is inextricably connected to the development of hearing deficits while being a poor predictor for the RAM25-EFR$_{PtN}$ amplitude, which we believe captures individual degrees of synaptopathy based on our model simulations and results from animal physiology studies.

The role of synaptopathy in predicting the SRT$_{SiQ\text{-}HP}$

Our model simulations and KA-manipulations support a causal relationship between synaptopathy and the RAM25-EFR$_{PtN}$. Consequently, the observed relationship between the RAM25-EFR$_{PtN}$ and SRT$_{SiN\text{-}HP}$ points to an important role of synaptopathy for speech recognition in noise. However, speech recognition in quiet does not necessarily depend solely on the ability to extract speech envelopes, especially given that the SRT$_{SiQ}$ strongly depends on audibility and OHC integrity (***Festen and Plomp, 1983***; ***Papakonstantinou et al., 2011***). Hence, in line with our synaptopathy-driven hypothesis #3, the predictive power of the RAM25-EFR$_{PtN}$ to the SRT$_{SiQ\text{-}HP}$ should be strongly reduced compared to the SRT$_{SiN\text{-}HP}$. We performed the same regression analysis as before to test this hypothesis for the SRT$_{SiQ\text{-}HP}$:

$$\mathrm{SRT_{SiQ\text{-}HP}} = \beta_0 + \beta_1 * \mathrm{RAM25\text{-}EFR_{PtN}} + \beta_2 * \mathrm{TH_{DPOAE,4kHz}} + \epsilon. \tag{5}$$

Table 2

Group	R^2	Adj. R^2	F (df_1,df_2)	p	beta	unique	common
ALL	0.57	0.55	27.57 (2,41)	<0.0001	β_1=-46.71*	8.67%	56.92%
					β_2=0.38***	34.42%	
NH$_{DP}$	0.29	0.21	3.34 (2,16)	0.061	β_1=-48.16	58.71%	24.88%
					β_2=0.19	16.41%	
OLD	0.31	0.26	5.81 (2,26)	0.008	β_1=7.33	0.21%	23.73%
					β_2=0.39**	76.06%	

Signif. codes: 0 '***' 0.001 '**' 0.01 '*' 0.05 '.' 0.1 ' ' 1

The regression model outcomes are summarized in Table 2 and confirm the predicted change of underlying SNHL mechanisms for speech recognition in quiet: the 4-kHz DPOAE threshold became the variable with the largest unique predictive power for the 'ALL' and OLD subgroups, while the common effect of the two explaining variables was comparable to that of the $SRT_{SiN\text{-}HP}$-model. The NH_{DP} model did not reach significance, supporting our hypothesis #3 and past observations that speech understanding in quiet relies on audibility rather than on TENV coding abilities.

Discussion

Understanding how different aspects of sensorineural hearing damage contribute to speech recognition deficits is still a major unsolved problem in hearing science, especially given the challenges associated with diagnosing synaptopathy non-invasively in humans (***Plack et al., 2016***; ***Hickox et al., 2017***; ***Kobel et al., 2017***; ***Bramhall et al., 2019***). We have to consider synaptopathy as an important facet of SNHL based on animal and human temporal bone studies of the progression of synaptopathy with age (***Sergeyenko et al., 2013***; ***Parthasarathy and Kujawa, 2018***; ***Wu et al., 2018***). This importance is further motivated by the observation that synaptopathy sets in before OHC damage after noise-exposure (e.g. ***Kujawa and Liberman, 2009***; ***Fernandez et al., 2015***), projecting its prevalence to largely exceed the 5.3% of world population estimated by the WHO, who suffer from a disabling hearing loss as diagnosed audiometrically (***Stevens et al., 2013***; ***WHO, 2019***).

This study minimized several aspects which, to date, have confounded the causal relationship between speech-in-noise intelligibility and synaptopathy in humans. Using a multiple regression and commonality analysis, we described to which degree two aspects of SNHL (synaptopathy and OHC-damage) were able to explain individual speech reception thresholds. Model-simulations and experimental findings provided theoretical and circumstantial evidence that the two variables included in the regression analysis can be treated as independent markers of OHC damage and synaptopathy, respectively. We considered a DPOAE threshold variable as a well-known marker of OHC damage (e.g. ***Davis et al., 2005***) and a RAM25-EFR_{PtN} variable as a marker for the individual degree of synaptopathy. Model simulations were crucial to the argument that the RAM25-EFR_{PtN} marker is maximally sensitive to synaptopathy, even in the presence of co-existing OHC deficits (***Vasilkov et al., 2020***). Computational frameworks offer an indispensable approach to understanding neural processing (***Einevoll et al., 2019***), as they uniquely can combine knowledge from imaging and physiology studies with non-invasive measures of brain function. Applied to this work, modeling the neuronal populations on the basis of EFR generation is - in the absence of available cochlear imaging techniques for living humans - the only existing technique that can establish how synaptopathy affects human EFR markers. On the basis of our model simulations and experimental modifications, we were able to establish relations between the RAM25-EFR_{PtN} amplitude and speech recognition performance in quiet and noise, in line with how cochlear synaptopathy is believed to affect auditory processing. We therefore conclude that age-related synaptopathy plays

an important role for speech intelligibility in noise.

Synaptopathy and speech intelligibility

Our RAM25-EFR results corroborate animal findings which relate deficits in temporal coding at the earliest neural stages of the auditory pathway to progressive/noise-induced cochlear synaptopathy (***Parthasarathy et al., 2014***; ***Fernandez et al., 2015***; ***Shaheen et al., 2015***; ***Parthasarathy and Kujawa, 2018***). Specifically, our results show an age-related decline in EFR amplitudes, even in the absence of OHC damage. The normal aging process results in a progressive decline in the number of ANFs, before OHC damage sets in (***Sergeyenko et al., 2013***; ***Möhrle et al., 2016***; ***Parthasarathy and Kujawa, 2018***) and human temporal bone studies confirm this trend (***Makary et al., 2011***; ***Wu et al., 2018***). By removing the low frequency content from the speech material to target TENV coding mechanisms, we may have exacerbated the compromising effect of synaptopathy on speech recognition, as it is well known that TENV information is crucial for speech comprehension (***Shannon et al., 1995***; ***Ding and Simon, 2012***). Our behavioral speech recognition results fell in line with this prediction, as the performance-difference between the oNH and oHI group decreased from the SiQ to SiN condition, but only for the high-pass filtered speech material (Fig. 7). Our hypothesis #3 which suggested a dominant effect of age-related synaptopathy on SiN recognition was further supported by the strong predictive power of the RAM25-EFR$_{PtN}$ metric on the high-pass, but not low-pass, filtered speech-in-noise test. Additionally, the SiQ condition was more strongly related to the 4-kHz DPOAE threshold as a proxy of OHC integrity.

The reason why earlier human studies of synaptopathy have drawn mixed conclusions regarding the relation between EFR strength as a marker of synaptopathy and speech intelligibility might in part be due to the low sensitivity of the classically used SAM-based EFR metrics (Figs. 3, 5, 8). We show that the RAM25-EFR shows an overall larger response, which is more strongly affected by KA-induced synaptopathy than the conventional SAM-EFR, which we earlier have shown to also be affected by OHC damage (***Vasilkov et al., 2020***). In addition, the mismatch in frequency content/coding mechanisms between the compared metrics in earlier studies might further explain the absence of significant effects among listeners with normal audiograms (***Grose et al., 2017***; ***Prendergast et al., 2017***; ***Guest et al., 2018***). Additionally, it is also likely that the effects of cochlear synaptopathy on auditory function are primarily present in populations with co-existing OHC dysfunction (***Bramhall et al., 2019***). This latter statement is supported by the fact that studies which included older participants or those with extreme noise-exposure histories tend to find electrophysiological evidence for synaptopathy or reduced temporal coding fidelity in the considered listener groups (e.g. ***Anderson et al., 2011***, ***2012***; ***Konrad-Martin et al., 2012***; ***Clinard and Tremblay, 2013***; ***Schoof and Rosen, 2016***; ***Bramhall et al., 2017***; ***Valderrama et al., 2018***). Within this context, our study confirms that age is inherently linked to the development of sensorineural hearing loss, but that the same age variable is a poor predictor of the synaptopathy degree in our age-restricted

samples (OLD, yNH).

Study limitations

Even though we show that the RAM25 metric captures synaptopathy-related variability, and that it plays a crucial role in maintaining normal speech recognition in noise as we age, it is important to note the limitations of our experimental approach.

(i) Present experimental limitations prevent us from establishing a direct relationship between synaptopathy and speech intelligibility in live humans and hence we need to rely on circumstantial evidence to support our conclusions. On the one hand, we used modeling to show how different SNHL pathologies affect the neuronal populations involved in the EFR generation, and on the other, we used an animal model to demonstrate the sensitivity of our EFR markers to synaptopathy. While the convergence of model and experimental results in several research studies (e.g. ***Verhulst et al., 2018b***; ***Keshishzadeh et al., 2019a***; ***Vasilkov et al., 2020***) lends credence to the validity of the model predictions for the purpose of this study, we need to keep in mind that state-of-the-art models are a good, but likely imperfect, representation of all neural mechanisms involved in EFR generation. At the same time, we need to consider that species differences might pose a confound to the direct comparison between budgerigar and human EFRs though neural recordings from the budgerigar inferior colliculus suggest shared processing strategies with the mammalian midbrain (***Henry et al., 2017***).

(ii) Significant correlations between the RAM25-EFR_{PtN} and $SRT_{SiN\text{-}HP}$ measures were only observed when pooling data from subgroups and thereby increasing the variance in outcome measures. Within the smaller groups (yNH, oNH, oHI), EFR-SRT relationships were only significant for the yNH group when excluding the two participants with elevated DPOAE thresholds (ρ = -0.57, p = 0.04, n = 13). The large EFR amplitude range in the yNH group corroborates findings in the animal model that show that synaptopathy can be exacerbated by noise exposure levels which do not cause OHC damage (***Fernandez et al., 2015***). The absence of significant EFR-SRT correlations within the older subgroups can be explained by the overall reported decline in EFR amplitudes with age (***Parthasarathy and Kujawa, 2018***; ***Dimitrijevic et al., 2016***), rendering it more difficult to observe coherent correlation trends between both metrics (Fig. 8).

(iii) All oNH participants had normal audiometric thresholds up to 4 kHz, and DPOAE thresholds confirmed that the observed threshold differences stemmed from OHC damage (Fig. 1 and 2). Nevertheless, the unfiltered and high-pass filtered speech material included speech energy beyond 4-kHz and recent work of ANF activity (***Henry et al., 2016***; ***Encina-Llamas et al., 2019***; ***Vasilkov and Verhulst, 2019***) has shown that for supra-threshold stimulation, TENV information can be encoded through the tails of high-SR ANF tuning curves at basal cochlear regions and contribute to EFR generation. Accounting for these potential confounds (e.g. through high-frequency masking noise) in future work might further strengthen the relationship between RAM25-EFR_{PtN} and speech

reception performance.

(iv) Pooling data from groups which differ in more than one factor can introduce additional explanatory between-group-factors that were not controlled for. For example, as it is known that cognitive factors such as memory and attention decrease with age and are linked to speech-in-noise understanding (***Humes et al., 2010***; ***Humes, 2013***; ***Yeend et al., 2017***), it is likely that some of the unaccounted variance can be attributed to these factors, especially as our analyses included groups with considerable age differences. Nevertheless, the matrix test is designed to minimize memory effects by randomly generating word sequences and by minimizing the cognitive load through immediate recall of just five words at a time. As EFR recordings to stimuli with high modulation frequencies are believed to be free from top-down attention (e.g. ***Varghese et al., 2015***) or memory effects, the strong correlations between the RAM25-EFR_{PtN} and $SRT_{SiN\text{-}HP}$ scores suggest that cognitive contributions are not a unique dominating factor, but rather interact with peripheral encoding deficits (***Johannesen et al., 2016***). We argue that for the purpose of this study, pooling of data from different homogeneous groups is a valid, and even necessary, approach to be able to disentangle the relative contributions of OHC damage and synaptopathy to speech intelligibility.

Conclusion

We conclude that age-related synaptopathy is an important hearing health issue, as we provide experimental and theoretical evidence that it strongly affects auditory TENV coding and speech intelligibility in noise. Sensitive hearing diagnostics is the first and most important step towards understanding the role of synaptopathy for impaired sound perception. The adopted RAM25-EFR marker was robust, widely applicable and selective for cochlear synaptopathy, and enabled us to draw our conclusions. With the established finding that synaptopathy is involved in speech perception, we can begin to develop therapeutic interventions aimed to compensate for the functional consequences of synaptopathy.

Conflict of interest statement

Ghent University filed a patent application (PCTEP2020053192) which covers some of the ideas presented in this paper. Sarah Verhulst and Viacheslav Vasilkov are inventors.

Acknowledgments

This work was supported by the DFG Cluster of Excellence EXC 1077/1 "Hearing4all" (MG, MM, SV), the European Research Council (ERC) under the Horizon 2020 Research and Innovation Programme (grant agreement No 678120 RobSpear; VV, SV), National Institutes of Health grant R01 DC017519 (KH) and a National Institutes of Health Predoctoral National Research Service Award Fellowship (TL1 TR002000) administered by the University of Rochester Clinical and Translational Science Institute (JW).

The authors would like to thank the study participants as well as the Hörzentrum Oldenburg for helping with participant recruitment.

Author Contributions

MG: Conceptualization, Methodology, Software, Validation, Formal analysis, Investigation, Data Curation, Writing: Original Draft, Visualization; VV: Methodology, Software, Investigation; MM: Methodology, Software, Investigation; JW: Methodology, Software, Investigation; KH: Methodology, Software, Investigation; SV: Conceptualization, Methodology, Investigation, Resources, Writing: Original Draft, Writing: Review & Editing, Supervision, Project administration, Funding acquisition.

Data Availability

The model code used for the simulations is available via 10.5281/zenodo.3717800 or github.com/HearingTec
The dataset is available upon reasonable request from the authors.

References

Altoè A, Pulkki V, Verhulst S. Transmission line cochlear models: improved accuracy and efficiency. The Journal of the Acoustical Society of America. 2014 Oct; 136(4):EL302–308. doi: 10.1121/1.4896416.

Altoè A, Pulkki V, Verhulst S. The effects of the activation of the inner-hair-cell basolateral K+ channels on auditory nerve responses. Hearing Research. 2018; 364:68–80. doi: 10.1016/j.heares.2018.03.029.

Anderson S, Parbery-Clark A, White-Schwoch T, Kraus N. Aging affects neural precision of speech encoding. The Journal of Neuroscience. 2012 Oct; 32(41):14156–14164. doi: 10.1523/JNEUROSCI.2176-12.2012.

Anderson S, Parbery-Clark A, Yi HG, Kraus N. A neural basis of speech-in-noise perception in older adults. Ear and Hearing. 2011 Dec; 32(6):750–757. doi: 10.1097/AUD.0b013e31822229d3.

Bharadwaj HM, Masud S, Mehraei G, Verhulst S, Shinn-Cunningham BG. Individual differences reveal correlates of hidden hearing deficits. The Journal of Neuroscience. 2015 Feb; 35(5):2161–2172. doi: 10.1523/JNEUROSCI.3915-14.2015.

Bledsoe SC, Bobbin RP, Chihal DM. Kainic acid: an evaluation of its action on cochlear potentials. Hearing Research. 1981 Mar; 4(1):109–120. doi: 10.1016/0378-5955(81)90040-x.

Boege P, Janssen T. Pure-tone threshold estimation from extrapolated distortion product otoacoustic emission I/O-functions in normal and cochlear hearing loss ears. The Journal of the Acoustical Society of America. 2002 Apr; 111(4):1810–1818. doi: 10.1121/1.1460923.

Bramhall N, Beach EF, Epp B, Le Prell CG, Lopez-Poveda EA, Plack CJ, Schaette R, Verhulst S, Canlon B. The search for noise-induced cochlear synaptopathy in humans: Mission impossible? Hearing Research. 2019 Mar; 377:88–103. doi: 10.1016/j.heares.2019.02.016.

Bramhall NF, Konrad-Martin D, McMillan GP, Griest SE. Auditory Brainstem Response Altered in Humans With Noise Exposure Despite Normal Outer Hair Cell Function. Ear and Hearing. 2017 Feb; 38(1):e1–e12. doi: 10.1097/AUD.0000000000000370.

Brand T, Kollmeier B. Efficient adaptive procedures for threshold and concurrent slope estimates for psychophysics and speech intelligibility tests. The Journal of the Acoustical Society of America. 2002 Jun; 111(6):2801–2810. doi: 10.1121/1.1479152.

Clinard CG, Tremblay KL. Aging degrades the neural encoding of simple and complex sounds in the human brainstem. Journal of the American Academy of Audiology. 2013 Aug; 24(7):590–599; quiz 643–644. doi: 10.3766/jaaa.24.7.7.

Costalupes JA, Young ED, Gibson DJ. Effects of continuous noise backgrounds on rate response of auditory nerve fibers in cat. Journal of Neurophysiology. 1984 Jun; 51(6):1326–1344. doi: 10.1152/jn.1984.51.6.1326.

Davis B, Qiu W, Hamernik RP. Sensitivity of distortion product otoacoustic emissions in noise-exposed chinchillas. Journal of the American Academy of Audiology. 2005 Feb; 16(2):69–78. doi: 10.3766/jaaa.16.2.2.

Dent ML, Dooling RJ, Pierce AS. Frequency discrimination in budgerigars (Melopsittacus undulatus): effects of tone duration and tonal context. The Journal of the Acoustical Society of America. 2000 May; 107(5 Pt 1):2657–2664. doi: 10.1121/1.428651.

Dimitrijevic A, Alsamri J, John MS, Purcell D, George S, Zeng FG. Human Envelope Following Responses to Amplitude Modulation: Effects of Aging and Modulation Depth. Ear and Hearing. 2016 Oct; 37(5):e322–335. doi: 10.1097/AUD.0000000000000324.

Ding N, Simon JZ. Emergence of neural encoding of auditory objects while listening to competing speakers. Proceedings of the National Academy of Sciences of the United States of America. 2012 Jul; 109(29):11854–11859. doi: 10.1073/pnas.1205381109.

Dolphin WF, Mountain DC. The envelope following response: scalp potentials elicited in the Mongolian gerbil using sinusoidally AM acoustic signals. Hearing Research. 1992 Feb; 58(1):70–78. doi: 10.1016/0378-5955(92)90010-K.

Dooling RJ, Lohr B, Dent ML. Hearing in Birds and Reptiles. In: Dooling RJ, Fay RR, Popper AN, editors. *Comparative Hearing: Birds and Reptiles* Springer Handbook of Auditory Research, New York, NY: Springer; 2000.p. 308–359. https://doi.org/10.1007/978-1-4612-1182-2_7, doi: 10.1007/978-1-4612-1182-2_7.

Dreyer A, Delgutte B. Phase locking of auditory-nerve fibers to the envelopes of high-frequency sounds: implications for sound localization. Journal of Neurophysiology. 2006 Nov; 96(5):2327–2341. doi: 10.1152/jn.00326.2006.

Dupont C, Horner J, Li C, Liu Q, Shepherd B, PResiduals: Probability-Scale Residuals and Residual Correlations; 2018. https://CRAN.R-project.org/package=PResiduals.

Einevoll GT, Destexhe A, Diesmann M, Grün S, Jirsa V, de Kamps M, Migliore M, Ness TV, Plesser HE, Schürmann F. The Scientific Case for Brain Simulations. Neuron. 2019 May; 102(4):735–744. doi: 10.1016/j.neuron.2019.03.027.

Encina-Llamas G, Harte JM, Dau T, Shinn-Cunningham B, Epp B. Investigating the Effect of Cochlear Synaptopathy on Envelope Following Responses Using a Model of the Auditory Nerve. Journal of the Association for Research in Otolaryngology: JARO. 2019 May; 20(4):363–382. doi: 10.1007/s10162-019-00721-7.

Fernandez KA, Jeffers PWC, Lall K, Liberman MC, Kujawa SG. Aging after noise exposure: acceleration of cochlear synaptopathy in "recovered" ears. The Journal of Neuroscience. 2015 May; 35(19):7509–7520. doi: 10.1523/JNEUROSCI.5138-14.2015.

Festen JM, Plomp R. Relations between auditory functions in impaired hearing. The Journal of the Acoustical Society of America. 1983 Feb; 73(2):652–662. doi: 10.1121/1.388957.

Furman AC, Kujawa SG, Liberman MC. Noise-induced cochlear neuropathy is selective for fibers with low spontaneous rates. Journal of Neurophysiology. 2013 Aug; 110(3):577–586. doi: 10.1152/jn.00164.2013.

Garrett M, Verhulst S. Applicability of subcortical EEG metrics of synaptopathy to older listeners with impaired audiograms. Hearing Research. 2019 Sep; 380:150–165. doi: 10.1016/j.heares.2019.07.001.

Glasberg BR, Moore BC. Auditory filter shapes in subjects with unilateral and bilateral cochlear impairments. The Journal of the Acoustical Society of America. 1986 Apr; 79(4):1020–1033. doi: 10.1121/1.393374.

Gramfort A, Luessi M, Larson E, Engemann DA, Strohmeier D, Brodbeck C, Goj R, Jas M, Brooks T, Parkkonen L, Hämäläinen M. MEG and EEG data analysis with MNE-Python. Frontiers in Neuroscience. 2013 Dec; 7:267. doi: 10.3389/fnins.2013.00267.

Gramfort A, Luessi M, Larson E, Engemann DA, Strohmeier D, Brodbeck C, Parkkonen L, Hämäläinen MS. MNE software for processing MEG and EEG data. NeuroImage. 2014 Feb; 86:446–460. doi: 10.1016/j.neuroimage.2013.10.027.

Greenwood DD. A cochlear frequency-position function for several species—29 years later. The Journal of the Acoustical Society of America. 1990; 87(6):2592–2605. doi: 10.1121/1.399052.

Grose JH, Buss E, Hall JW. Loud Music Exposure and Cochlear Synaptopathy in Young Adults: Isolated Auditory Brainstem Response Effects but No Perceptual Consequences. Trends in Hearing. 2017 Jan; 21:2331216517737417. doi: 10.1177/2331216517737417.

Guest H, Munro KJ, Prendergast G, Millman RE, Plack CJ. Impaired speech perception in noise with a normal audiogram: No evidence for cochlear synaptopathy and no relation to lifetime noise exposure. Hearing Research. 2018; 364:142–151. doi: 10.1016/j.heares.2018.03.008.

Henry KS, Abrams KS. Persistent Auditory Nerve Damage Following Kainic Acid Excitotoxicity in the Budgerigar (Melopsittacus undulatus). Journal of the Association for Research in Otolaryngology: JARO. 2018; 19(4):435–449. doi: 10.1007/s10162-018-0671-y.

Henry KS, Abrams KS, Forst J, Mender MJ, Neilans EG, Idrobo F, Carney LH. Midbrain Synchrony to Envelope Structure Supports Behavioral Sensitivity to Single-Formant Vowel-Like Sounds in Noise. Journal of the Association for Research in Otolaryngology: JARO. 2017 Feb; 18(1):165–181. doi: 10.1007/s10162-016-0594-4.

Henry KS, Kale S, Heinz MG. Distorted Tonotopic Coding of Temporal Envelope and Fine Structure with Noise-Induced Hearing Loss. The Journal of Neuroscience. 2016 Feb; 36(7):2227–2237. doi: 10.1523/JNEUROSCI.3944-15.2016.

Hickox AE, Larsen E, Heinz MG, Shinobu L, Whitton JP. Translational issues in cochlear synaptopathy. Hearing Research. 2017 Jun; 349:164–171. doi: 10.1016/j.heares.2016.12.010.

Hoben R, Easow G, Pevzner S, Parker MA. Outer Hair Cell and Auditory Nerve Function in Speech Recognition in Quiet and in Background Noise. Frontiers in Neuroscience. 2017; 11. doi: 10.3389/fnins.2017.00157.

Holmes E, Griffiths TD. 'Normal' hearing thresholds and fundamental auditory grouping processes predict difficulties with speech-in-noise perception. Scientific Reports. 2019 Nov; 9(1):16771. doi: 10.1038/s41598-019-53353-5.

Hopkins K, Moore B, Stone M. Effects of moderate cochlear hearing loss on the ability to benefit from temporal fine structure information in speech. The Journal of the Acoustical Society of America. 2008 Mar; 123:1140–53. doi: 10.1121/1.2824018.

Hopkins K, Moore BCJ. The importance of temporal fine structure information in speech at different spectral regions for normal-hearing and hearing-impaired subjects. The Journal of the Acoustical Society of America. 2010 Mar; 127(3):1595–1608. doi: 10.1121/1.3293003.

Huet A, Batrel C, Tang Y, Desmadryl G, Wang J, Puel JL, Bourien J. Sound coding in the auditory nerve of gerbils. Hearing Research. 2016; 338:32–39. doi: 10.1016/j.heares.2016.05.006.

Humes LE. Understanding the speech-understanding problems of older adults. American Journal of Audiology. 2013 Dec; 22(2):303–305. doi: 10.1044/1059-0889(2013/12-0066).

Humes LE, Kewley-Port D, Fogerty D, Kinney D. Measures of Hearing Threshold and Temporal Processing across the Adult Lifespan. Hearing research. 2010 Jun; 264(1-2):30–40. doi: 10.1016/j.heares.2009.09.010.

Humphrey R, Playrec, Multi-channel Matlab Audio; 2008. http://www.playrec.co.uk.

ISO. Acoustics - Statistical distribution of hearing thresholds related to age and gender (7029). Switzerland: International Organization of Standardization, ISO; 2017. https://www.iso.org/standard/42916.html.

Johannesen PT, Buzo BC, Lopez-Poveda EA. Evidence for age-related cochlear synaptopathy in humans unconnected to speech-in-noise intelligibility deficits. Hearing Research. 2019 Mar; 374:35–48. doi: 10.1016/j.heares.2019.01.017.

Johannesen PT, Pérez-González P, Kalluri S, Blanco JL, Lopez-Poveda EA. The Influence of Cochlear Mechanical Dysfunction, Temporal Processing Deficits, and Age on the Intelligibility of Audible Speech in Noise for Hearing-Impaired Listeners. Trends in Hearing. 2016 Jan; 20:2331216516641055. doi: 10.1177/2331216516641055.

Joris PX, Yin TC. Responses to amplitude-modulated tones in the auditory nerve of the cat. The Journal of the Acoustical Society of America. 1992 Jan; 91(1):215–232. doi: 10.1121/1.402757.

Joris PX, Verschooten E. On the limit of neural phase locking to fine structure in humans. Advances in Experimental Medicine and Biology. 2013; 787:101–108. doi: 10.1007/978-1-4614-1590-9_12.

Keshishzadeh S, Garrett M, Vasilkov V, Verhulst S. The Derived-Band Envelope Following Response and its Sensitivity to Sensorineural Hearing Deficits. bioRxiv. 2019; doi: 10.1101/820704.

Keshishzadeh S, Vasilkov V, Verhulst S. Tonotopic Sensitivity to Supra-threshold Hearing Deficits of the Envelope Following Response Evoked by Broadband Stimuli. In: *Proceedings of the ICA 2019 and EAA Euroregio* Aachen; 2019. http://pub.dega-akustik.de/ICA2019/data/articles/001145.pdf.

Kim S. ppcor: An R Package for a Fast Calculation to Semi-partial Correlation Coefficients. Communications for statistical applications and methods. 2015 Nov; 22(6):665–674. doi: 10.5351/CSAM.2015.22.6.665.

Kobel M, Le Prell CG, Liu J, Hawks JW, Bao J. Noise-induced cochlear synaptopathy: Past findings and future studies. Hearing Research. 2017 Jun; 349:148–154. doi: 10.1016/j.heares.2016.12.008.

Konrad-Martin D, Dille MF, McMillan G, Griest S, McDermott D, Fausti SA, Austin DF. Age-related changes in the auditory brainstem response. Journal of the American Academy of Audiology. 2012 Jan; 23(1):18–75. doi: 10.3766/jaaa.23.1.3.

Kraus N, Anderson S, White-Schwoch T. The Frequency-Following Response: A Window into Human Communication. In: *The Frequency-Following Response: A Window into Human Communication*; 2017.p. 1–15. doi: 10.1007/978-3-319-47944-6_1.

Kujawa SG, Liberman MC. Adding insult to injury: cochlear nerve degeneration after "temporary" noise-induced hearing loss. The Journal of Neuroscience. 2009 Nov; 29(45):14077–14085. doi: 10.1523/JNEUROSCI.2845-09.2009.

Kummer P, Janssen T, Arnold W. The level and growth behavior of the 2 f1-f2 distortion product otoacoustic emission and its relationship to auditory sensitivity in normal hearing and cochlear hearing loss. The Journal of the Acoustical Society of America. 1998 Jun; 103(6):3431–3444. doi: 10.1121/1.423054.

Kuwada S, Anderson JS, Batra R, Fitzpatrick DC, Teissier N, D'Angelo WR. Sources of the scalp-recorded amplitude-modulation following response. Journal of the American Academy of Audiology. 2002; 13(4):188–204.

Le Prell CG. Effects of noise exposure on auditory brainstem response and speech-in-noise tasks: a review of the literature. International Journal of Audiology. 2019 Feb; 58(sup1):S3–S32. doi: 10.1080/14992027.2018.1534010.

Liberman MC. Auditory-nerve response from cats raised in a low-noise chamber. The Journal of the Acoustical Society of America. 1978 Feb; 63(2):442–455. doi: 10.1121/1.381736.

Lin FR, Thorpe R, Gordon-Salant S, Ferrucci L. Hearing loss prevalence and risk factors among older adults in the United States. The Journals of Gerontology Series A, Biological Sciences and Medical Sciences. 2011 May; 66(5):582–590. doi: 10.1093/gerona/glr002.

Long GR, Talmadge CL, Lee J. Measuring distortion product otoacoustic emissions using continuously sweeping primaries. The Journal of the Acoustical Society of America. 2008 Sep; 124(3):1613–1626. doi: 10.1121/1.2949505.

Lopez-Poveda EA. Why do I hear but not understand? Stochastic undersampling as a model of degraded neural encoding of speech. Frontiers in Neuroscience. 2014 Oct; 8. doi: 10.3389/fnins.2014.00348.

Lopez-Poveda EA, Barrios P. Perception of stochastically undersampled sound waveforms: a model of auditory deafferentation. Frontiers in Neuroscience. 2013; 7:124. doi: 10.3389/fnins.2013.00124.

Lorenzi C, Gilbert G, Carn H, Garnier S, Moore BCJ. Speech perception problems of the hearing impaired reflect inability to use temporal fine structure. Proceedings of the National Academy of Sciences of the United States of America. 2006 Dec; 103(49):18866–18869. doi: 10.1073/pnas.0607364103.

Makary CA, Shin J, Kujawa SG, Liberman MC, Merchant SN. Age-related primary cochlear neuronal degeneration in human temporal bones. Journal of the Association for Research in Otolaryngology: JARO. 2011 Dec; 12(6):711–717. doi: 10.1007/s10162-011-0283-2.

Marmel F, Rodríguez-Mendoza MA, Lopez-Poveda EA. Stochastic undersampling steepens auditory threshold/duration functions: implications for understanding auditory deafferentation and aging. Frontiers in Aging Neuroscience. 2015; 7:63. doi: 10.3389/fnagi.2015.00063.

Mauermann M. Improving the usability of the distortion product otoacoustic emisssions (DPOAE)-sweep method: An alternative artifact rejection and noise-floor estimation. The Journal of the Acoustical Society of America. 2013 May; 133:3376. doi: 10.1121/1.4805803.

Mauermann M, Kollmeier B. Distortion product otoacoustic emission (DPOAE) input/output functions and the influence of the second DPOAE source. The Journal of the Acoustical Society of America. 2004 Oct; 116(4 Pt 1):2199–2212. doi: 10.1121/1.1791719.

Mehraei G, Hickox AE, Bharadwaj HM, Goldberg H, Verhulst S, Liberman MC, Shinn-Cunningham BG. Auditory Brainstem Response Latency in Noise as a Marker of Cochlear Synaptopathy. The Journal of Neuroscience. 2016 Mar; 36(13):3755–3764. doi: 10.1523/JNEUROSCI.4460-15.2016.

Millman KJ, Aivazis M. Python for Scientists and Engineers. Computing in Science Engineering. 2011 Mar; 13(2):9–12. doi: 10.1109/MCSE.2011.36.

Mitchell C, Phillips DS, Trune DR. Variables affecting the auditory brainstem response: audiogram, age, gender and head size. Hearing Research. 1989 Jun; 40(1-2):75–85. doi: 10.1016/0378-5955(89)90101-9.

Möhrle D, Ni K, Varakina K, Bing D, Lee SC, Zimmermann U, Knipper M, Rüttiger L. Loss of auditory sensitivity from inner hair cell synaptopathy can be centrally compensated in the young but not old brain. Neurobiology of Aging. 2016 Aug; 44:173–184. doi: 10.1016/j.neurobiolaging.2016.05.001.

Neely ST, Johnson TA, Kopun J, Dierking DM, Gorga MP. Distortion-product otoacoustic emission input/output characteristics in normal-hearing and hearing-impaired human ears. The Journal of the Acoustical Society of America. 2009 Aug; 126(2):728–738. doi: 10.1121/1.3158859.

Nelson PC, Carney LH. A phenomenological model of peripheral and central neural responses to amplitude-modulated tones. The Journal of the Acoustical Society of America. 2004 Oct; 116(4 Pt 1):2173–2186. doi: 10.1121/1.1784442.

Newton RG, Spurrell DJ. A Development of Multiple Regression for the Analysis of Routine Data. Journal of the Royal Statistical Society: Series C (Applied Statistics). 1967; 16(1):51–64. doi: 10.2307/2985237.

Nimon K, Lewis M, Kane R, Haynes RM. An R package to compute commonality coefficients in the multiple regression case: an introduction to the package and a practical example. Behavior Research Methods. 2008 May; 40(2):457–466. doi: 10.3758/BRM.40.2.457.

Oliphant TE. Python for Scientific Computing. Computing in Science Engineering. 2007 May; 9(3):10–20. doi: 10.1109/MCSE.2007.58.

Osses Vecchi A, Verhulst S. Calibration and reference simulations for the auditory periphery model of Verhulst et al. 2018 version 1.2. arXiv e-prints. 2019 Dec; p. arXiv:1912.10026. https://ui.adsabs.harvard.edu/abs/2019arXiv191210026O.

Papakonstantinou A, Strelcyk O, Dau T. Relations between perceptual measures of temporal processing, auditory-evoked brainstem responses and speech intelligibility in noise. Hearing Research. 2011 Oct; 280(1-2):30–37. doi: 10.1016/j.heares.2011.02.005.

Parthasarathy A, Datta J, Torres JAL, Hopkins C, Bartlett EL. Age-related changes in the relationship between auditory brainstem responses and envelope-following responses. Journal of the Association for Research in Otolaryngology: JARO. 2014 Aug; 15(4):649–661. doi: 10.1007/s10162-014-0460-1.

Parthasarathy A, Kujawa SG. Synaptopathy in the Aging Cochlea: Characterizing Early-Neural Deficits in Auditory Temporal Envelope Processing. The Journal of Neuroscience. 2018 Aug; 38(32):7108–7119. doi: 10.1523/JNEUROSCI.3240-17.2018.

Picton TW. Human Auditory Evoked Potentials. Plural Publishing; 2010.

Plack CJ, Léger A, Prendergast G, Kluk K, Guest H, Munro KJ. Toward a Diagnostic Test for Hidden Hearing Loss. Trends in Hearing. 2016 Sep; 20. doi: 10.1177/2331216516657466.

Prendergast G, Millman RE, Guest H, Munro KJ, Kluk K, Dewey RS, Hall DA, Heinz MG, Plack CJ. Effects of noise exposure on young adults with normal audiograms II: Behavioral measures. Hearing Research. 2017 Dec; 356:74–86. doi: 10.1016/j.heares.2017.10.007.

Pujol R, Lenoir M, Robertson D, Eybalin M, Johnstone BM. Kainic acid selectively alters auditory dendrites connected with cochlear inner hair cells. Hearing Research. 1985 May; 18(2):145–151. doi: 10.1016/0378-5955(85)90006-1.

R Core Team, R: A language and environment for statistical computing. Vienna, Austria: R Foundation for Statistical Computing; 2019. https://www.R-project.org/.

Ray-Mukherjee J, Nimon K, Mukherjee S, Morris DW, Slotow R, Hamer M. Using commonality analysis in multiple regressions: a tool to decompose regression effects in the face of multicollinearity. Methods in Ecology and Evolution. 2014; 5(4):320–328. doi: 10.1111/2041-210X.12166.

Russell V. Least-Squares Means: The R Package lsmeans. Journal of Statistical Software. 2016; 69(1):1–33. doi: doi:10.18637/jss.v069.i01.

Schmiedt RA, Mills JH, Boettcher FA. Age-related loss of activity of auditory-nerve fibers. Journal of Neurophysiology. 1996 Oct; 76(4):2799–2803. doi: 10.1152/jn.1996.76.4.2799.

Schoof T, Rosen S. The Role of Age-Related Declines in Subcortical Auditory Processing in Speech Perception in Noise. Journal of the Association for Research in Otolaryngology: JARO. 2016 Oct; 17(5):441–460. doi: 10.1007/s10162-016-0564-x.

Sergeyenko Y, Lall K, Liberman MC, Kujawa SG. Age-related cochlear synaptopathy: an early-onset contributor to auditory functional decline. The Journal of Neuroscience. 2013 Aug; 33(34):13686–13694. doi: 10.1523/JNEUROSCI.1783-13.2013.

Shaheen LA, Valero MD, Liberman MC. Towards a Diagnosis of Cochlear Neuropathy with Envelope Following Responses. Journal of the Association for Research in Otolaryngology: JARO. 2015 Dec; 16(6):727–745. doi: 10.1007/s10162-015-0539-3.

Shannon RV, Zeng FG, Kamath V, Wygonski J, Ekelid M. Speech recognition with primarily temporal cues. Science. 1995 Oct; 270(5234):303–304. doi: 10.1126/science.270.5234.303.

Shera CA, Guinan JJ, Oxenham AJ. Otoacoustic estimation of cochlear tuning: validation in the chinchilla. Journal of the Association for Research in Otolaryngology: JARO. 2010 Sep; 11(3):343–365. doi: 10.1007/s10162-010-0217-4.

Stevens G, Flaxman S, Brunskill E, Mascarenhas M, Mathers CD, Finucane M, Global Burden of Disease Hearing Loss Expert Group. Global and regional hearing impairment prevalence: an analysis of 42 studies in 29 countries. European Journal of Public Health. 2013 Feb; 23(1):146–152. doi: 10.1093/eurpub/ckr176.

Sun H, Hashino E, Ding DL, Salvi RJ. Reversible and irreversible damage to cochlear afferent neurons by kainic acid excitotoxicity. The Journal of Comparative Neurology. 2001 Feb; 430(2):172–181. doi: 10.1002/1096-9861(20010205)430:2<172::aid-cne1023>3.0.co;2-w.

Sun H, Salvi RJ, Ding DL, Hashino DE, Shero M, Zheng XY. Excitotoxic effect of kainic acid on chicken otoacoustic emissions and cochlear potentials. The Journal of the Acoustical Society of America. 2000 Apr; 107(4):2136–2142. doi: 10.1121/1.428495.

Trune DR, Mitchell C, Phillips DS. The relative importance of head size, gender and age on the auditory brainstem response. Hearing Research. 1988 Mar; 32(2-3):165–174. doi: 10.1016/0378-5955(88)90088-3.

Valderrama JT, Beach EF, Yeend I, Sharma M, Van Dun B, Dillon H. Effects of lifetime noise exposure on the middle-age human auditory brainstem response, tinnitus and speech-in-noise intelligibility. Hearing Research. 2018 Aug; 365:36–48. doi: 10.1016/j.heares.2018.06.003.

Varghese L, Bharadwaj HM, Shinn-Cunningham BG. Evidence against attentional state modulating scalp-recorded auditory brainstem steady-state responses. Brain Research. 2015 Nov; 1626:146–164. doi: 10.1016/j.brainres.2015.06.038.

Vasilkov V, Garrett M, Mauermann M, Verhulst S. Enhancing the sensitivity of the envelope-following response for cochlear synaptopathy screening in humans: the role of stimulus envelope. bioRxiv. 2020 Jan; p. 2020.06.05.136184. http://biorxiv.org/content/early/2020/06/05/2020.06.05.136184.abstract, doi: 10.1101/2020.06.05.136184.

Vasilkov V, Verhulst S. Towards a differential diagnosis of cochlear synaptopathy and outer-hair-cell deficits in mixed sensorineural hearing loss pathologies. medRxiv. 2019; doi: 10.1101/19008680.

Verhulst S, Altoè A, Vasilkov V. Computational modeling of the human auditory periphery: Auditory-nerve responses, evoked potentials and hearing loss. Hearing Research. 2018 Mar; 360:55–75. doi: 10.1016/j.heares.2017.12.018.

Verhulst S, Dau T, Shera CA. Nonlinear time-domain cochlear model for transient stimulation and human otoacoustic emission. The Journal of the Acoustical Society of America. 2012 Dec; 132(6):3842–3848. doi: 10.1121/1.4763989.

Verhulst S, Ernst F, Garrett M, Vasilkov V. Supra-threshold psychoacoustics and envelope-following response relations: normal-hearing, synaptopathy and cochlear gain loss. Acta Acustica united with Acustica. 2018; 104(5):800–803. doi: 10.3813/AAA.919227.

Verhulst S, Jagadeesh A, Mauermann M, Ernst F. Individual Differences in Auditory Brainstem Response Wave Characteristics: Relations to Different Aspects of Peripheral Hearing Loss. Trends in Hearing. 2016 Nov; 20:1–20. doi: 10.1177/2331216516672186.

Verhulst S, Warzybok A. Contributions of Low- and High-Frequency Sensorineural Hearing Deficits to Speech Intelligibility in Noise. bioRxiv. 2019; doi: 10.1101/358127.

Verschooten E, Robles L, Joris PX. Assessment of the limits of neural phase-locking using mass potentials. The Journal of Neuroscience: The Official Journal of the Society for Neuroscience. 2015 Feb; 35(5):2255–2268. doi: 10.1523/JNEUROSCI.2979-14.2015.

Viana LM, O'Malley JT, Burgess BJ, Jones DD, Oliveira CACP, Santos F, Merchant SN, Liberman LD, Liberman MC. Cochlear neuropathy in human presbycusis: Confocal analysis of hidden hearing loss in post-mortem tissue. Hearing Research. 2015 Sep; 327:78–88. doi: 10.1016/j.heares.2015.04.014.

Wagener KC, Kühnel V, Kollmeier B. Entwicklung und Evaluation eines Satztests für die deutsche Sprache III: Evaluation des Oldenburger Satztests. Zeitschrift für Audiologie / Audiological Acoustics. 1999; 38(3):86–95.

WHO, Deafness and hearing loss; 2019. https://www.who.int/news-room/fact-sheets/detail/deafness-and-hearing-loss.

Wong SJ, Abrams KS, Amburgey KN, Wang Y, Henry KS. Effects of selective auditory-nerve damage on the behavioral audiogram and temporal integration in the budgerigar. Hearing Research. 2019; 374:24–34. doi: 10.1016/j.heares.2019.01.019.

Wu PZ, Liberman LD, Bennett K, de Gruttola V, O'Malley JT, Liberman MC. Primary Neural Degeneration in the Human Cochlea: Evidence for Hidden Hearing Loss in the Aging Ear. Neuroscience. 2018 Aug; 407:8–20. doi: 10.1016/j.neuroscience.2018.07.053.

Yeend I, Beach EF, Sharma M, Dillon H. The effects of noise exposure and musical training on suprathreshold auditory processing and speech perception in noise. Hearing Research. 2017; 353:224–236. doi: 10.1016/j.heares.2017.07.006.

Zheng XY, Henderson D, Hu BH, McFadden SL. Recovery of structure and function of inner ear afferent synapses following kainic acid excitotoxicity. Hearing Research. 1997 Mar; 105(1-2):65–76. doi: 10.1016/s0378-5955(96)00188-8.

Zhu L, Bharadwaj H, Xia J, Shinn-Cunningham B. A comparison of spectral magnitude and phase-locking value analyses of the frequency-following response to complex tones. The Journal of the Acoustical Society of America. 2013 Jul; 134(1):384–395. doi: 10.1121/1.4807498.

Figure captions

Figure 1: Pure-tone hearing thresholds (dB HL) at frequencies between 0.125-8 kHz. Groups are split based on audiometric loss and age (yNH: young normal-hearing, oNH: old normal-hearing, oHI: old hearing impaired). Thick traces with error-bands represent the group mean and standard deviation per frequency. Thin traces represent individual audiogram profiles. The box centered around the 4-kHz mark, shows the frequency region of the SAM tone stimulus including side bands (4 ± 0.12 kHz).

Figure 2: Boxplots and individual data points of the pure-tone audiometric thresholds and distortion product otoacoustic emissions at 4 kHz for all groups (yNH, oNH, oHI).

Figure 3: **A,B**) Two cycles of the SAM and RAM25 stimuli used for EFR recording. **C,D**) Simulated summed responses from maximally 19 auditory nerve fibers with different spontaneous firing rates (SR; H: high-SR, M: medium-SR, L: low-SR) at 4-kHz CF in response to the stimuli depicted in **A** and **B**. Three hearing profiles are shown: NH - no hearing deficits, HI_{synap} - simulated synaptopathy (reduced number of fibers) and HI_{flat} - 35 dB hearing loss across all frequencies. **E,F**) Two averaged cycles (over all available pairs of cycles (15) in the averaged bootstrapped EFR waveform) in response to the stimuli depicted in **A,B** respectively but with a modulation frequency of 100 Hz and modulation depth of 100%. The data shown are from one of the budgerigars (K20) before and twelve weeks after the administration of kainic acid.

Figure 4: Schematic of the EFR_{PtN} computation process per bootstrap run, based on the averaged yNH RAM25 data. **A)** Extraction of the PtN magnitudes (vertical arrows) for the modulation frequency and its first four harmonics (h_0-h_4) from the averaged spectral estimate of the neural frequency responses (F_n). Orange lines indicate the respective noise floor levels (NFs) for each considered frequency. **B)** Reconstructed time-domain wave form based on the five frequency components (h_0-h_4) and their respective phases. The orange dashed line shows how the EFR_{PtN} amplitude is lastly extracted from the averaged bootstrapped wave forms (W_b).

Figure 5: **A**) Simulated EFR_{PtN} amplitudes for the NH and HI_{flat} profiles for both stimulus types and varying degrees of synaptopathy (varying numbers of SR fiber types). **B**) Boxplots and individual data points of the measured EFR_{PtN} amplitudes for both stimulus types and three participant groups (yNH, oNH, oHI). **C**) EFR_{PtN} amplitudes from two budgerigars (K20, K25) at two time points before and four, six, eight and twelve weeks after the administration of kainic acid.

Figure 6: Regression plots of the EFR_{PtN} amplitudes and DPOAE thresholds at 4 kHz for both EFR stimulus types (**A,B**: SAM, **C,D**: RAM25) and two participant subgroups (**A,C**: NH_{DP}, **B,D**: HI_{DP}).

Groups are color-coded according to their age (Young, Old). Error bars at the bottom of each panel indicate mean and standard deviation for young and old participants.

Figure 7: Boxplots and individual data points of the speech recognition thresholds (SRT_{50}) of the German matrix test for all groups (yNH, oNH, oHI). Speech-in-quiet (SiQ) results for all three filter conditions (BB: broadband, LP: 1.5 kHz low-pass, HP: 1.65 kHz high-pass) are show in **A**. Speech-in-noise (SiN) results for all filter conditions are depicted in **B**. Lines between boxplots per group visualize group-mean profiles.

Figure 8: Regression plots of the EFR_{PtN} amplitudes of both stimulus types (**A,B,C**: SAM, **D,E,F**: RAM25) and SRT_{50} measure for the broadband (**A,D**), low-pass (**B/E**) and high-pass filtered condition (**C/F**). Groups (yNH, oNH, oHI) are color-coded and correlation coefficients are depicted in each panel for 'ALL' participants and two subgroups (NH_{DP}, OLD).

Table captions

Table 1: Summary of the multiple linear regression models and commonality analyses predicting high-pass filtered speech-in-noise performance ($SRT_{SiN\text{-}HP}$) using the RAM25-EFR_{PtN} (β_1) and 4-kHz DPOAE thresholds (β_2) for 'ALL' participants and two subgroups (NH_{DP}, OLD). Commonality coefficients describe the fraction of the model's total explained variance (R^2) uniquely and commonly accounted for by the predictor variables.

Table 2: Summary of the multiple linear regression models and commonality analyses predicting high-pass filtered speech-in-quiet performance ($SRT_{SiQ\text{-}HP}$) using the RAM25-EFR_{PtN} (β_1) and 4-kHz DPOAE thresholds (β_2) for 'ALL' participants and two subgroups (NH_{DP}, OLD). Commonality coefficients describe the fraction of the model's total explained variance (R^2) uniquely and commonly accounted for by the predictor variables.

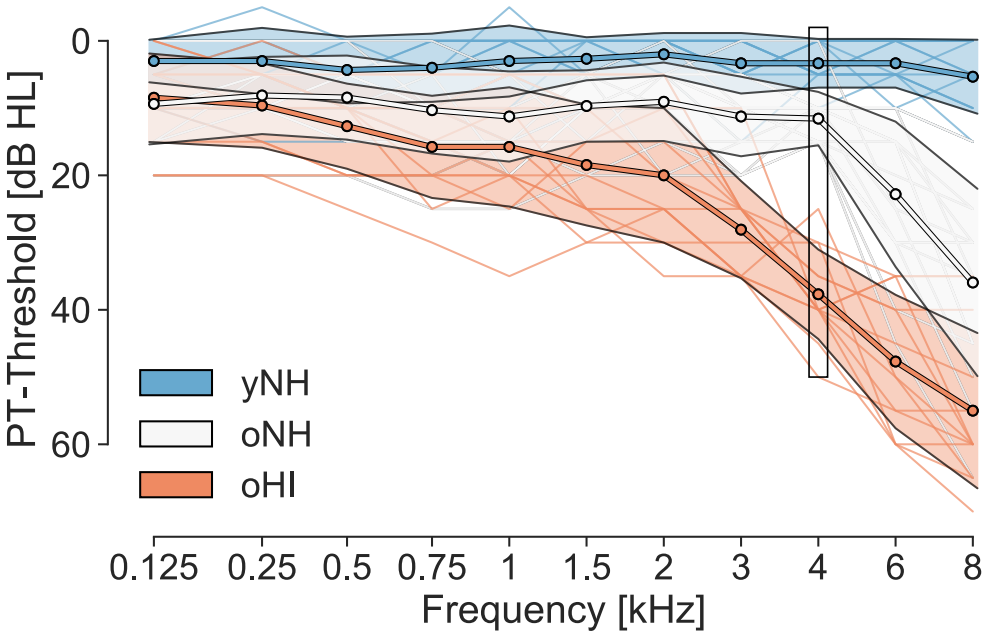

Figure 1

Figures

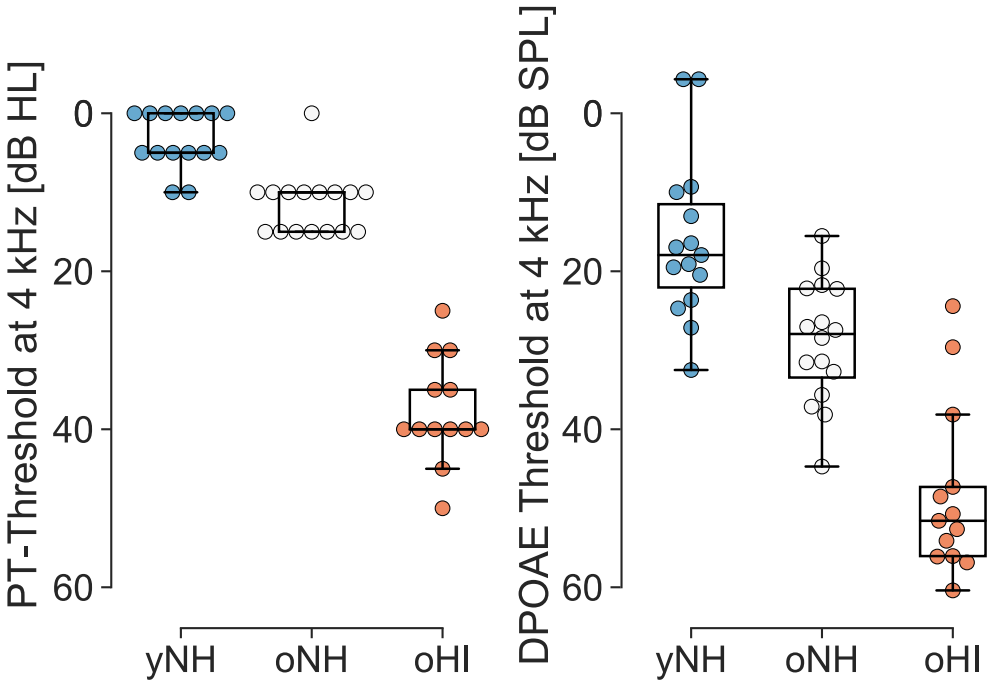
PT-Threshold at 4 kHz [dB HL]
0
20
40
60
yNH
oNH
oHI
DPOAE Threshold at 4 kHz [dB SPL]
0
20
40
60
yNH
oNH
oHI

Figure 2

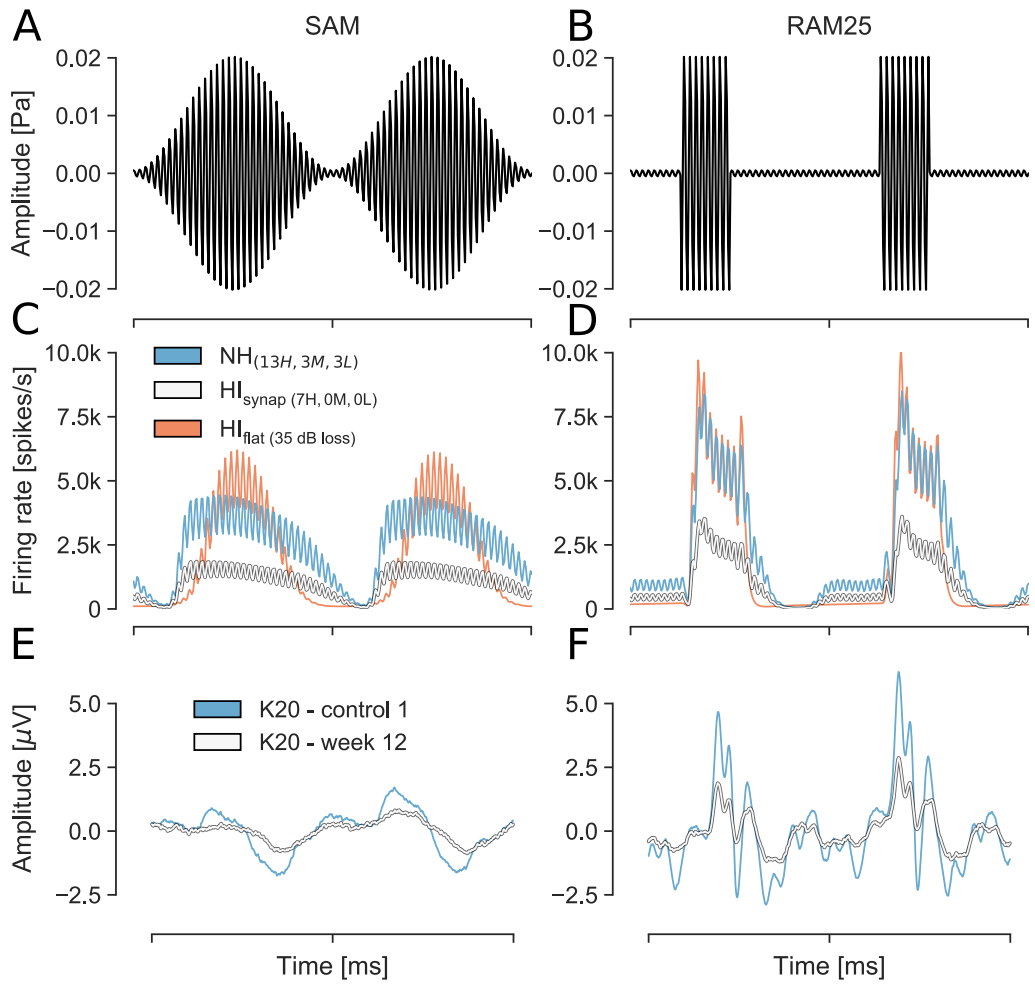

Figure 3

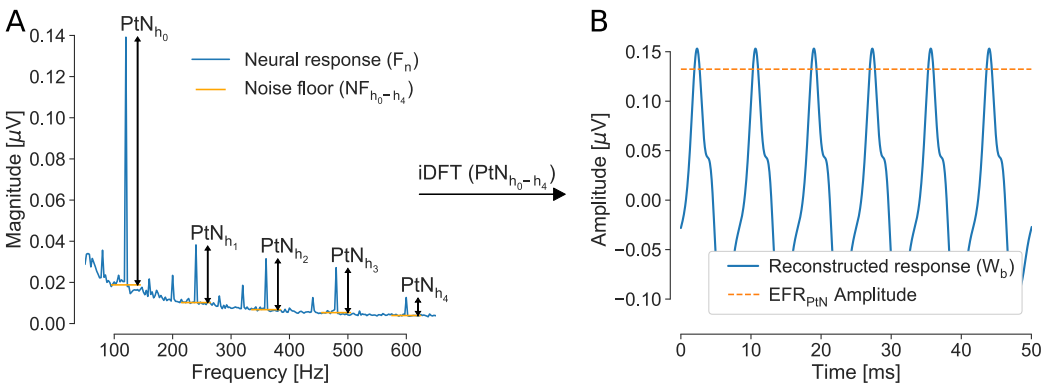

Figure 4

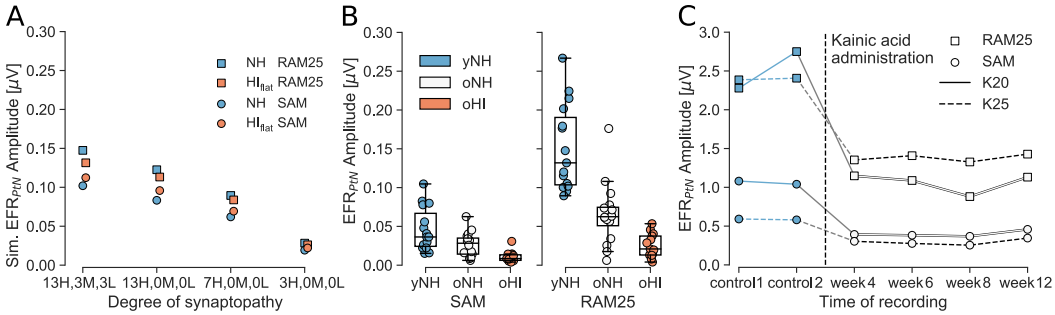

Figure 5

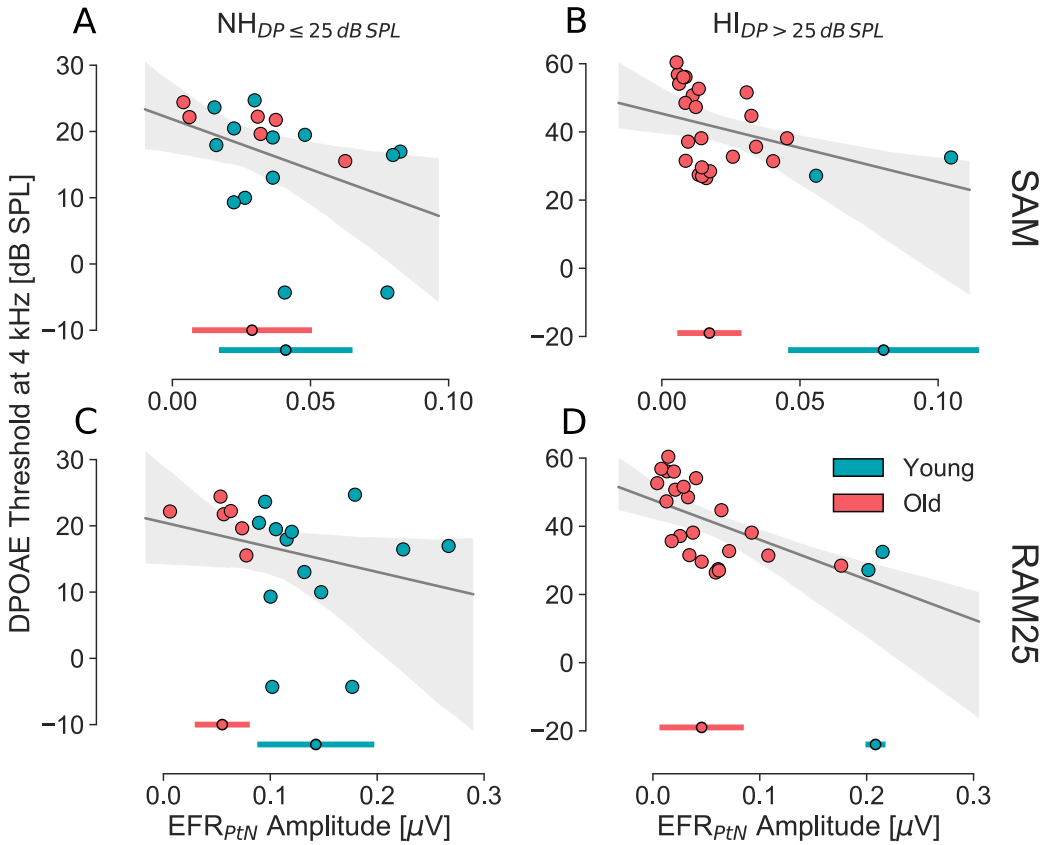

Figure 6

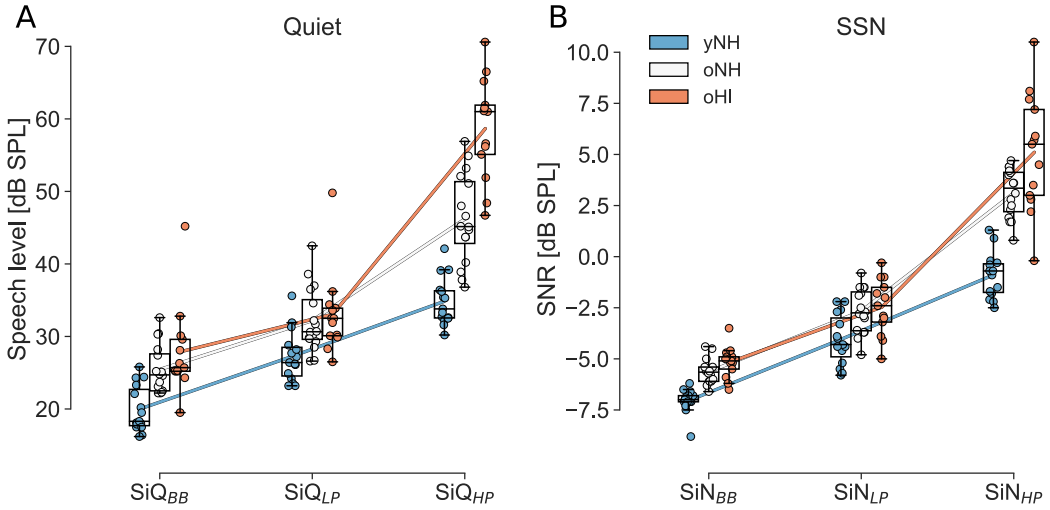

Figure 7

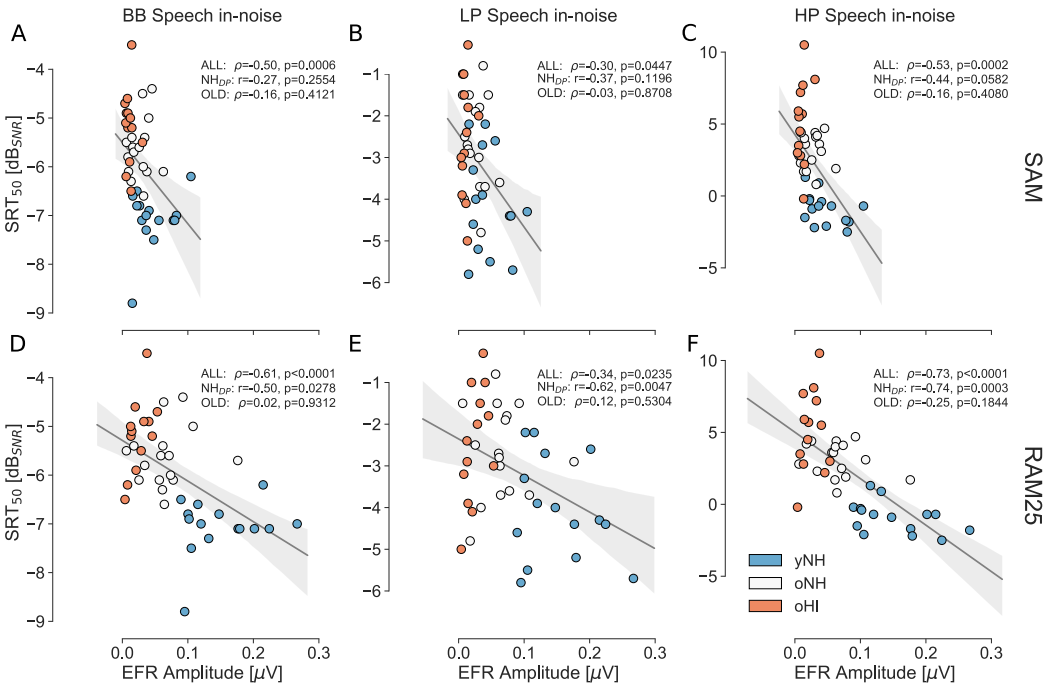

Figure 8